

**NEW METHODS FOR CAPACITIVE WIRELESS
POWER TRANSFER**

By

SU CHOON CHUNG

A dissertation submitted to the Department of Electrical and Electronic Engineering,
Faculty of Engineering and Science,
Universiti Tunku Abdul Rahman,
in partial fulfillment of the requirements for the degree of
Master of Engineering Science
September 2013

ABSTRACT

NEW METHODS FOR CAPACITIVE WIRELESS POWER TRANSFER

Su Choon Chung

Nowadays, it is a trend to deploy wireless mechanism in most modern communication systems because of its numerous advantages such as flexibility movement of the communicating devices and the ease of communication system build-up in remote areas. However, the current communication devices have to be powered-up via electrical connections. The motivation of achieving fully wireless communication systems prompts the interests to explore the wireless power transfer (WPT) mechanism for such systems. WPT has the distinct advantage in evading electrical shock as compared to the conventional electrical connections due to the electrical isolation between the power supply and the devices. This dissertation focuses on the utilization of uni-directional capacitive coupling of electric field between metallic plates for efficient capacitive WPT (CWPT) within their near-field distance. It is divided into three parts in which a new CWPT model will be introduced in each part. They are intended for WPT over a mid-range distance and on-chip and small-device applications.

In the first part, a novel method for CWPT is demonstrated through the use of a pair of parallel metallic plates associated with their respective ground plates. It has been found that the parallel plates are able to produce a better power transfer efficiency (PTE) and much wider bandwidth than a pair of conventional coils in the same frequency range. The uni-directional of the electric fields between parallel plates plays the instrumental role in producing such advantages for the plates over the coils. The frequency characteristics and the design flexibilities of the model are studied in detail. Two arrays of 2×2 elements of the novel CWPT model are designed using the identical model to investigate the PTE and frequency characteristics of the simultaneous power transfer of multiple WPT elements placed in a near distance between each other. This model is applicable to many practical communication systems and electrical appliances such as medical implant and car battery charging. The measurement results agree well with the results simulated by using CST Microwave Studio.

Next, by embedding a pair of parallel plates inside another pair, all of equal size, another new CWPT model is proposed. In this model, the power is supplied to the outer pair of plates and received by the inner pair. Such a structure allows effective confinement of electric field used for power transfer within the field exchanging medium between the power transmitting plates. It is necessary for an efficient WPT. A simple but yet efficient $50\text{-}\Omega$ input and output impedances transformation scheme has been associated to the model by using a pair of capacitors. This model is intended for embedded small devices applications.

Finally, the model explored in the first part is used for transferring power to a chip placed on top of a PCB via wireless mechanism. The entire chip is represented by a piece of substrate. The power receiving plate on the chip can either be attached to the bottom layer of the chip or be embedded inside it. The experimental results agree well with the simulation results. The PTE and the dielectric breakdown voltages of the model have been analyzed and discussed. A series of characteristic investigations have been done on the model by simulations.

As the current trend of designing various modern wireless communication systems and electrical appliances emphasizes on electrical safety and portability, the CWPT models introduced in this dissertation should be able to provide solutions. With the rapid increase in operating frequency of the contemporary microwave circuits, wireless mechanism can be a potential alternative for on-chip power transfer in the future. This is because metallic interconnects are no longer efficient in very high frequency ranges.

ACKNOWLEDGEMENT

First of all, I would like to express my deepest gratitude to my dissertation supervisor, *Dr. Lim Eng Hock* for his guidance throughout my studies. With his sincere and patient encouragements, my research works go on smoothly. Also, thanks for providing me the research assistantship to pursue my studies in UTAR.

Besides, I am grateful to my co-supervisor, *Prof. Chung Boon Kuan* for his useful advises and consultations. Special thanks to the staffs in the Telecommunication Laboratory of UTAR for their assistance in performing my research works.

Finally, appreciation is given to all my family members who always support and encourage me.

APPROVAL SHEET

This dissertation entitled “**NEW METHODS FOR CAPACITIVE WIRELESS POWER TRANSFER**” was prepared by SU CHOON CHUNG and submitted as partial fulfillment of the requirements for the degree of Master of Engineering Science at Universiti Tunku Abdul Rahman.

Approved by:

(Assist. Prof. Dr. LIM ENG HOCK)

Date:.....

Supervisor

Department of Electrical and Electronics Engineering

Faculty of Engineering and Science

Universiti Tunku Abdul Rahman

(Prof. Dr. CHUNG BOON KUAN)

Date:.....

Co-supervisor

Department of Electrical and Electronics Engineering

Faculty of Engineering and Science

Universiti Tunku Abdul Rahman

**FACULTY OF ENGINEERING AND SCIENCE
UNIVERSITI TUNKU ABDUL RAHMAN**

Date: _____

SUBMISSION OF DISSERTATION

It is hereby certified that **SU CHOON CHUNG** (ID No: **10UEM07346**) has completed this dissertation entitled “NEW METHODS FOR CAPACITIVE WIRELESS POWER TRANSFER” under the supervision of Dr. Lim Eng Hock (Supervisor) from the Department of Electrical and Electronics Engineering, Faculty of Engineering and Science, and Prof. Dr. Chung Boon Kuan (Co-Supervisor) from the Department of Electrical and Electronics Engineering, Faculty of Engineering and Science.

I hereby give permission to my supervisors to write and prepare a manuscript of these research findings for publishing in any form, if I did not prepare it within six (6) months time from this date, provided, that my name is included as one of the authors for this article. Arrangement of names will depend on my supervisors.

DECLARATION

I hereby declare that the dissertation is based on my original work except for quotations and citations which have been duly acknowledged. I also declare that it has not been previously or concurrently submitted for any other degree at UTAR or other institutions.

Name : _____

Date : _____

TABLE OF CONTENTS

ABSTRACT	ii
ACKNOWLEDGEMENT	v
APPROVAL SHEET	vi
SUBMISSION SHEET	vii
DECLARATION	viii
TABLE OF CONTENTS	ix
LIST OF TABLES	xi
LIST OF FIGURES	xii
LIST OF ABBREVIATIONS	xv

CHAPTER

1	INTRODUCTION AND BACKGROUND	1
1.1	Background of Wireless Power Transfer Technologies	1
1.2	Brief Introduction of Capacitive Wireless Power Transfer	6
1.3	Motivation and Contributions	8
1.4	Outline of the Dissertation	9
2	MID-RANGE CAPACITIVE WIRELESS POWER TRANSFER	11
2.1	Introduction	11
2.2	Wireless Power Transfer Mechanism	11
2.2.1	Inductive Wireless Power Transfer	12
2.2.2	Capacitive Wireless Power Transfer	13
2.3	Capacitive Wireless Power Transfer Configuration	14
2.3.1	Design and Optimization	16
2.3.2	Power Transfer Efficiency	17

2.4	Results and Discussions	18
2.4.1	Separation Distance	18
2.4.2	Parametric Analysis for CWPT	24
2.4.3	2 × 2 Array for CWPT	27
2.5	Conclusion	31
3	WIRELESS POWER TRANSFER FOR MOTHERBOARD PERIPHERALS	32
3.1	Introduction	32
3.2	Model Configuration	34
3.2.1	Electric Field Mechanism	36
3.2.2	Impedance Matching	37
3.3	Results and Discussion	38
3.4	Conclusion	52
4	CAPACITIVE WIRELESS POWER TRANSFER FOR ON-CHIP APPLICATIONS	53
4.1	Introduction	53
4.2	Capacitive Wireless Power Transfer Configuration	54
4.3	Results and Discussion	57
4.3.1	Power Transfer Efficiency	57
4.3.2	Dielectric Breakdown Voltage	60
4.3.3	Studies on Impedance and Power Transmission	62
4.4	Conclusion	72
5	SUMMARY AND FUTURE WORK	73
5.1	Summary	73
5.2	Future Work	74

References

LIST OF TABLES

TABLES	TITLE	PAGE
Table 3.1:	Measured and simulated $ S_{21} $, PTE, and operating frequencies of the equal plates configuration ($L_1 = L_2 = 15\text{cm}$) at different d values.	43
Table 3.2:	Capacitances used for different values of d for the equal parallel plates configuration ($L_1 = L_2 = 15\text{cm}$).	43
Table 3.3:	Measured and simulated impedances of the equal plates configuration ($L_1 = L_2 = 15\text{cm}$) at different d : (a) Input impedance. (b) Output impedance.	45

LIST OF FIGURES

FIGURES	TITLE	PAGE
Figure 2.1:	Magnetic flux coupling between two coils.	13
Figure 2.2:	CWPT via electric field coupling between two parallel plates.	14
Figure 2.3:	The proposed CWPT method by using a pair of parallel plates. Also shown are their respective ground plates.	15
Figure 2.4:	Inductive wireless power transfer demonstrated by a pair of rectangular coils. It is designed to have the same frequency as that for CWPT in Fig. 2.3.	16
Figure 2.5:	Comparison of the performances of the plates and coils: (a) Maximum coupling coefficient. (b) Reflection coefficient $ S_{11} $ at max $ S_{21} $. The respective operating frequencies are also shown in the figures.	20
Figure 2.6:	Comparison of the PTE for the CWPT and coils.	21
Figure 2.7:	The measured and simulated S parameters and input impedance at $d = 0.5\text{cm}$: (a) CWPT. (b) Coils.	22
Figure 2.8:	Operating frequency and the corresponding maximum $ S_{21} $ of the CWPT as a function of the plate-to-ground distance D .	25
Figure 2.9:	Operating frequency and the corresponding maximum $ S_{21} $ of the coils as a function of the coil height h , with $d = 10\text{ cm}$.	26
Figure 2.10:	Operating frequency and the corresponding maximum $ S_{21} $ of the CWPT as a function of ground size L .	27
Figure 2.11:	A 2×2 array for the CWPT.	28

Figure 2.12:	Total received current (I_a) and operating frequency of the 2×2 CWPT as a function of d . Also given is the current of the single-plate (I_s).	30
Figure 2.13:	Total received current as a function of W . Also given is its corresponding operating frequency.	31
Figure 3.1:	Peripheral printed circuit boards inside a computer casing.	33
Figure 3.2:	The proposed power transfer schemes for chips and ICs on the peripheral boards.	33
Figure 3.3:	Experiment setup for demonstrating the proposed power transfer schemes for chips and ICs.	36
Figure 3.4:	The network model of the proposed parallel plates system: (a) Without matching capacitor. (b) With matching capacitors.	38
Figure 3.5:	Measured and simulated S parameters for the equal plates ($L_1 = L_2 = 15\text{cm}$) at $d = 0.5\text{cm}$ and $D = 0.5\text{cm}$.	39
Figure 3.6:	Measured and simulated impedances of the equal plates at $d = 0.5\text{cm}$ and $D = 0.5\text{cm}$: (a) Input impedance. (b) Output impedance.	41
Figure 3.7:	Effect of C_1 on the equal plates configuration ($L_1 = L_2 = 15\text{cm}$): (a) Input and output impedances. (b) Maximum $ S_{21} $ and operating frequencies.	48
Figure 3.8:	Effect of C_2 on the equal plates configuration ($L_1 = L_2 = 15\text{cm}$): (a) Input and output impedances. (b) Maximum $ S_{21} $ and operating frequencies.	49
Figure 3.9:	Measured and simulated S parameters for the parallel plates with $L_1 = 15\text{cm}$, $L_2 = 7.5\text{cm}$, $d = 1\text{cm}$, and $D = 0.5\text{cm}$. The corresponding measured and simulated input impedances are shown in the inset.	51
Figure 3.10:	Photograph showing the equal plates system ($L_1 = L_2 = 15\text{cm}$, $d = 0.5\text{cm}$, $D = 0.5\text{cm}$, and $C_1 = 39\text{pF}$, $C_2 = 47\text{pF}$) for lighting up LED.	52
Figure 4.1:	The proposed CWPT scheme for on-chip applications: (a) Profile view. (b) Top view.	55
Figure 4.2:	On-chip CWPT scheme with an embedded substrate between the patches.	56

Figure 4.3:	Simulated and measured S parameters of the CWPT model in Fig. 4.1. The inset shows the corresponding simulated and measured input impedances.	58
Figure 4.4:	Simulated and measured S parameters of the CWPT model with an embedded layer between the two patches (Fig. 4.2). The inset shows the corresponding simulated and measured input impedances.	59
Figure 4.5:	Effect of the load impedance Z_L on the maximum $ S_{21} $ and operating frequency of the CWPT in Fig. 4.1.	63
Figure 4.6:	Effect of the distance between patches d on the maximum $ S_{21} $ and operating frequency.	64
Figure 4.7:	Effect of plate size on the maximum $ S_{21} $ and operating frequency.	65
Figure 4.8:	Effect of chip material on the maximum $ S_{21} $ and operating frequency: (a) Relative dielectric constant ϵ_{rc} . (b) Thickness t .	66
Figure 4.9:	Effect of the ground size C_{g2} on the maximum $ S_{21} $ and operating frequency.	67
Figure 4.10:	Effect of the PCB material on the maximum $ S_{21} $ and operating frequency: (a) Relative dielectric constant ϵ_{rp} . (b) Thickness h .	69
Figure 4.11:	The effect of the dimension of the C-shaped slot on the maximum $ S_{21} $ and operating frequency: (a) P_1 . (b) P_2 .	71

LIST OF ABBREVIATIONS

CWPT	Capacitive wireless power transfer
IWPT	Inductive wireless power transfer
PTE	Power transfer efficiency
WPT	Wireless power transfer

CHAPTER 1

INTRODUCTION AND BACKGROUND

1.1 Background of Wireless Power Transfer Technologies

Wireless mechanism has long been used by many types of communication systems such as mobile phones, walkie-talkies, and cordless phones for the convenience of flexible movement. However, such devices are usually charged up by the traditional electrically wired power supplies. Recently, there has been increasing interest to explore wireless power transfer (WPT) mechanism as an alternative power scheme. With the use of wireless powering method, an electronic device can be charged up even if it is moving.

In the early 20th century, Nikola Tesla (1904a; 1904b; 1914) has made effort to transfer power via wireless mechanism. In the subsequent years, although no extensive attempts were made for the development of this technology, it has re-emerged in the 1960s. The development history of WPT technology since Nikola Tesla age was later summarized by N. Shinohara (2011b). In many applications, wireless power transfer is desirable due to the several advantages:

- (i) In electrical hazardous environment (e.g. high humidity, gas, dust), electrical connections may cause risky sparking and electrical shocks. These problems can

be avoided by using wireless mechanism since there is no physical contact between the power supply and device.

- (ii) Wireless mechanism allows more flexible and free movement of robots in production line.
- (iii) Avoidance of loose cables and the associated connectors during charging process and the replacement of batteries. Such incidences will cause disruption to the operation of a movable or portable device charged-up through conventional electrical connections.
- (iv) Medical implants (e.g. pacemakers) can be charged up without involving risky medical operation for the replacement of the batteries.

Transferring power in space is a great challenge as electromagnetic wave attenuates with distance. In the earliest stage, effort was made to achieve long-distance power transmission through far-field techniques (Dickinson 1976; Brown 1984; Brown and Eves 1992). However, the achievable power transfer efficiency (PTE) is very limited. In order to provide sufficient power to a satellite in space, huge power has to be supplied to the transmitter at the base station which could violate the RF safety regulations (IEEE 1999). Usually, the far-field techniques are only able to transfer very low power. Due to the rapid increase of energy consumption by the mankind, the source of energy in the earth is expected to deplete in the coming decades. As a solution, effort has been initiated to transfer solar energy, a renewable and sustainable energy, from solar power satellites to the earth using

microwave techniques (Matsumoto 2002; Mcspadden and Mankins 2002). High efficiency power amplifiers (Yamanaka et al., 2010) and active phased arrays with phase-controlled magnetrons (Shinohara et al., 2000) are developed to facilitate this technology.

In the past few years, several models and strategies have been proposed for efficient WPT in the near-field distance. In 2007, a group of physicists from Massachusetts Institute of Technology demonstrated a highly efficient WPT model via the strongly coupled magnetic resonance of a pair of coils (Kurs et al., 2007). In order to ensure maximum power delivery to the load, simultaneous adaptive optimal source and load impedances have to be applied in measurements. Obviously, this is not easy to be done practically. Instead, high PTE can also be achieved by applying frequency tracking approach with a fixed complex load matched at the maximum power delivery distance of interest (Park et al. 2011). This impedance matching method is much simpler but it is able to achieve a PTE that is close to the case of applying simultaneous adaptive input and output impedance matching. It can be seen from (Fu et al., 2009) that frequency tracking in a resonant coupling WPT system is critical in maximizing the PTE as the mutual inductance of the transmitting and receiving coils varies with the separation distance of the coils.

It has been shown that the insertion of an intermediate coil in between a pair of resonant coils, all are designed to have the same resonant frequency, can significantly improve the PTE and extend the distance of power delivery (Kim et al., 2011). The intermediate coil can be oriented coaxially or perpendicularly to the pair of coils, with the former performing better. The intermediate coil can also

substantially reduce the energy radiated from the pair of coils through an electromagnetically induced transparency-like scheme while improving its PTE (Hamam et al., 2009). In addition, a transponder-based WPT system can improve the PTE from the source to the load with a non-monotonic decay of PTE with respect to distance, with an extended operating range (Ettorre and Grbic 2012).

In the past, the WPT systems demonstrated by using the magnetically coupled coils are only efficient for power transfer within near-field and mid-range distances (Kalaris et al., 2008; Zhu et al., 2008; Kim et al., 2009; Low et al., 2009; Cheon et al., 2011; Azad et al., 2012). Such WPT models are usually limited to a certain fixed distance and orientation, with PTE drops drastically when the receiver is moved away from its optimal setting. Later, as desired by some applications, the WPT system with a nearly constant PTE over the strong magnetically coupled region can also be achieved through an automated frequency tuning scheme (Sample et al., 2011). In this case, the power transmitted to the receiver is almost constant regardless of its orientation and distance from the transmitter as long as it is still within the working range of the transmitter. The rapid development of WPT technology has spurred the interest of exploring simultaneous power transfer to multiple receivers (Cannon et al., 2009; Casanova et al., 2009; Kurs et al., 2010). It enables multiple wireless portable devices to be charged up simultaneously, a distinct advantage over the conventional wired charging schemes.

Besides the non-radiative mechanism, efficient WPT can also be achieved by using the electrically small folded cylindrical helix dipoles with high radiation efficiency (Yoon and Ling 2010). Various PTE optimization methods for antennas

have been analyzed in terms of load impedance, frequency tuning, geometry, and relative orientation between antennas, directivity, as well as the radiation efficiency of antennas (Kim and Ling 2007; Tak et al., 2009; Chen et al., 2010; Lee and Nam 2010; Tak et al., 2011; Park et al. 2012; Warnick et al., accepted for publication). Rectennas (antennas integrated with rectifier) can also be used for WPT (Brown 1980; Shinohara and Matsumoto 1998; Homma et al., 2011). A rectenna can be made into a duo-functional system for simultaneous wireless power transmission and communication (Shinohara 2011a). Effort has been made to improve the ac-dc conversion efficiency of the rectennas in order to minimize microwave power loss for a higher output power (Brown 1976; Bharj et al., 1992; Yoo and Chang 1992; Mcspadden et al., 1997; Hatano et al., 2011).

In recent years, WPT has been deployed in biomedical applications (Chow et al., 2011; RamRakhyani et al., 2011; Kim et al., 2012; Sun et al., 2012). Investigation shows that power transmission to body area network is feasible with a satisfactory PTE (Jeong et al., 2012). Charging up the medical implantable devices through wireless mechanism can avoid the battery-replacing medical surgery. This technology can facilitate the practical use of implantable devices and provide convenience to patients in the future. The use of WPT technology in capsule endoscopy is able to enhance the medical diagnostic and treatment capabilities for various diseases and health conditions (Park et al., 2008; Shiba et al., 2008; Sun et al., 2012). Besides, there was also investigation done on the wireless powering of sensors embedded in concrete (Jiang and Georgakopoulos 2012). The PTE is much affected by the electrical properties and moisture content of concrete.

Nowadays, microwave signals are easily available wherever RF communications are taking place. In addition to the dedicated usages, the energy carried by the ambient RF signals can also be further utilized by harvesting and converting them into direct current to power up electronic devices (Hagerty et al., 2004; Olgun et al., 2011).

In order to miniaturize the transmitter size for practical WPT applications, there is an increasing interest to transform and design various power transmitters on a planar surface (Tang et al., 2000; Hui and Ho 2005; Liu and Hui 2008). Such transmitters are potentially useful for charging up the portable electronic gadgets, such as mobile phones and MP3 players. It can also be used for simultaneous wireless signal and energy transfer as well as transferring power to multiple receivers. WPT also finds its potential applications in electric vehicles (Esser 1995; Wang et al., 2005; Imura et al., 2009), micro-robots (Mukhopadhyay et al., 2008), and portable-telephones (Jang and Jovanovic 2003).

1.2 Brief Introduction of Capacitive Wireless Power Transfer

Besides the inductive wireless power transfer (IWPT) scheme which uses magnetic field as the power transfer mechanism, capacitive wireless power transfer (CWPT) through electric field coupling between two pairs of parallel metallic plates has drawn much attention recently (Liu et al., 2009; Kline et al., 2010; Liu and Hu 2011). Comparing to IWPT, the CWPT method has much less field leakage. A CWPT system can be modeled by using extended stroboscopic mapping method

under steady state condition (Liu and Hu 2009; Liu et al., 2011). The zero-voltage switching operating frequencies and steady-state waveforms of the system can then be determined. In general, zero-voltage switching can be considered as square wave power utilizing a constant off-time control which varies the conversion frequency, or on-time to maintain regulation of the output voltage. It is usually employed in high-frequency resonant converter topologies to reduce switching losses.

The application of CWPT can be extended to 3-D VLSI. A particular case is the inter-chip bi-directional communication and power transfer between two stacked chips (Culurciello and Andreou 2006). It was the first demonstration of simultaneous wireless data and power transfer between chips in a stack. The integration of power telemetry and wireless data transfer through a capacitive coupling scheme was also done for medical implants (Sodagar and Amiri 2009). As the electric field used for capacitive power transfer is confined inside two plates, it does not interfere with the neighbouring circuitries. Therefore, multiple telemetry links can be established at the same frequency.

The output power of a CWPT system can be increased by exciting it with a multi-stage switched mode active negative capacitor (Fnato et al., 2010). The PTE can be improved without LC resonance, making it robust against parameter change. Therefore, no frequency tracking scheme is required for such system. The CWPT technology can also be potentially deployed for charging up respiratory devices (Zheng et al., 2010) and soccer-playing robots (Hu et al., 2008).

1.3 Motivation and Contributions

This dissertation aims at exploring new methods for realizing capacitive wireless power transfer (CWPT) for a better power transfer efficiency (PTE). It utilizes the uni-directional electric field coupling between the parallel plates. In the first part, a novel scheme for CWPT is proposed by using only a pair of parallel metallic plates, effectively eliminating the need of two pairs of parallel plates in the conventional CWPT systems. The pair of parallel plates is made up by a power transmitting plate and a power receiving plate. A ground plate is associated with each of the plates functioning as the complimentary path to form a closed-loop circuit. This model can be potentially used for charging up electronic devices over a mid-range distance.

The second part of the dissertation provides a wireless powering alternative for the peripherals on a motherboard. It is designed by embedding a pair of parallel plates inside another. The AC power supplied to the outer pair of plates can later be received by the inner ones. The received power is then channelled to the electronic devices connected to the plates.

Finally, two on-chip WPT schemes have been demonstrated in this dissertation. These methods make use of the CWPT configuration proposed in *Chapter 2* for transferring wireless power to a chip placed on top of a printed circuit board (PCB). In the future, it can potentially provide a feasible solution for transferring power on-chip at a very high frequency where metallic interconnects become inefficient.

1.4 Outline of the Dissertation

This dissertation introduces three capacitive wireless power transfer (CWPT) configurations based on the uni-directional electric field coupling between metallic plates. The previous works done on exploring and investigating the WPT technologies have been described in *Chapter 1*. Various WPT schemes and applications have been explained and compared. The recent development of the CWPT technology is briefly summarized.

In *Chapter 2*, a new CWPT configuration will be introduced for mid-range WPT. Simulations and experiments have been carried out to compare the power transfer efficiency (PTE) of the newly proposed CWPT structure with that of conventional coils. Finally, simultaneous power transfer of the 2×2 CWPT array is explored.

In *Chapter 3*, two new CWPT schemes have been proposed for sending wireless power to computer peripherals. Power transfer to the capacitive patches on both the chip package and PCB substrate has been explored here. The PTE is studied for two different cases. In the first, power transfer between two equal plates is investigated. The second one explores sending electric power from a pair of large plates to another of smaller size.

In *Chapter 4*, with the use of the CWPT model proposed in *Chapter 2*, the idea of transferring power to a chip placed on a PCB through wireless mechanism is

presented. The capacitive patch can be made either on top or embedded inside the chip package. A series of simulations and experiments have been conducted to study the operating frequency and PTE.

Chapter 5 concludes the dissertation, together with the recommendations and discussions for further research.

CHAPTER 2

MID-RANGE CAPACITIVE WIRELESS POWER TRANSFER

2.1 Introduction

In this chapter, the uni-directional electric field between a pair of parallel plates is deployed for wireless power transfer (WPT). The power transfer efficiency of the proposed plates is compared to the conventional inductive coils where energy is transfer through magnetic induction. A new method is introduced for optimizing the WPT models for a more efficient power transmission. The bandwidth of the proposed structure is also compared to that for coils. Studies have been conducted to study the design flexibility of the proposed CWPT model. Two 2×2 CWPT arrays are designed and their characteristics is compared to that of single element.

2.2 Wireless Power Transfer Mechanism

In this section, two different types of wireless power transfers will be studied for their field distributions. The first part, the conventional magnetic induction is deployed for transferring power wirelessly and the properties are studied. Second part compares the proposed capacitive wireless power transfer (CWPT) with the coils.

In this chapter, the coupling mechanism, power transmission, and parametric studies of the coils and plates will be analyzed.

2.2.1 Inductive Wireless Power Transfer

Magnetic field is one type of physical mechanism that can be used for transferring power wirelessly. To do that, as shown in Fig. 2.1, a pair of current-carrying metallic coils is usually deployed for generating and sensing the magnetic flux lines. Alternating current is supplied to the primary coil for generating magnetic field, with its flux distribution shown in Fig. 2.1. As can be seen, the flux lines around the primary coil are similar to those of a simple bar magnet. It is the strongest at the center point of the coil and reduces with distance. A secondary coil is then aligned in parallel to the primary to couple its fluxes. Current will then be generated in the secondary coil. This is the reverse process of magnetic field generation. As can be seen in Fig. 2.1, the field distribution around the two coils is similar to the case where two magnets are aligned facing each other with the opposite polarity. The field strength sensed by the second coil reduces with the increase in separation distance. This protocol is usually suitable for mid-range distance at low frequencies.

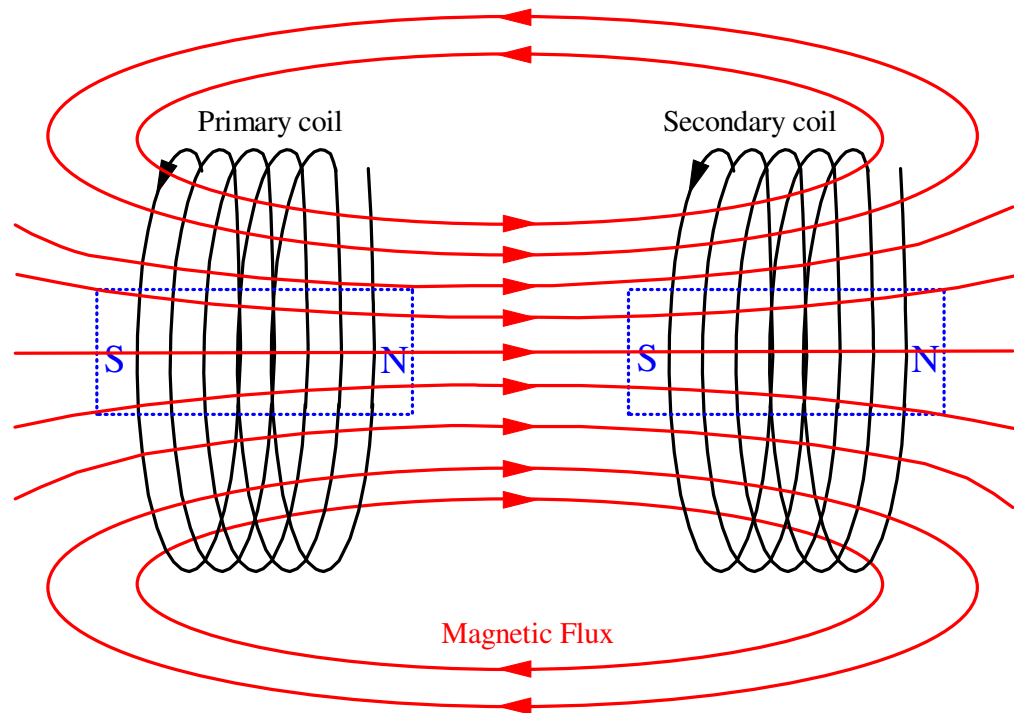


Figure 2.1: Magnetic flux coupling between two coils.

2.2.2 Capacitive Wireless Power Transfer

Capacitive wireless power transfer (CWPT) method utilizes the electric field coupling mechanism for transferring power wirelessly. Here, electric fluxes are usually generated by a pair of metallic plates, as shown in Fig. 2.2. As can be seen from the figure, electric flux is uni-directional as it starts from the transmitting plate (positively polarized) and ends at the inner surface of the receiving plate (negatively polarized). This property remains unaffected regardless of the distance between the two plates. In practice, the electric field lines near the edges of the plates can become slightly distorted due to fringing fields. The characteristics of the parallel plates here are quite similar to those for the parallel-plate capacitor.

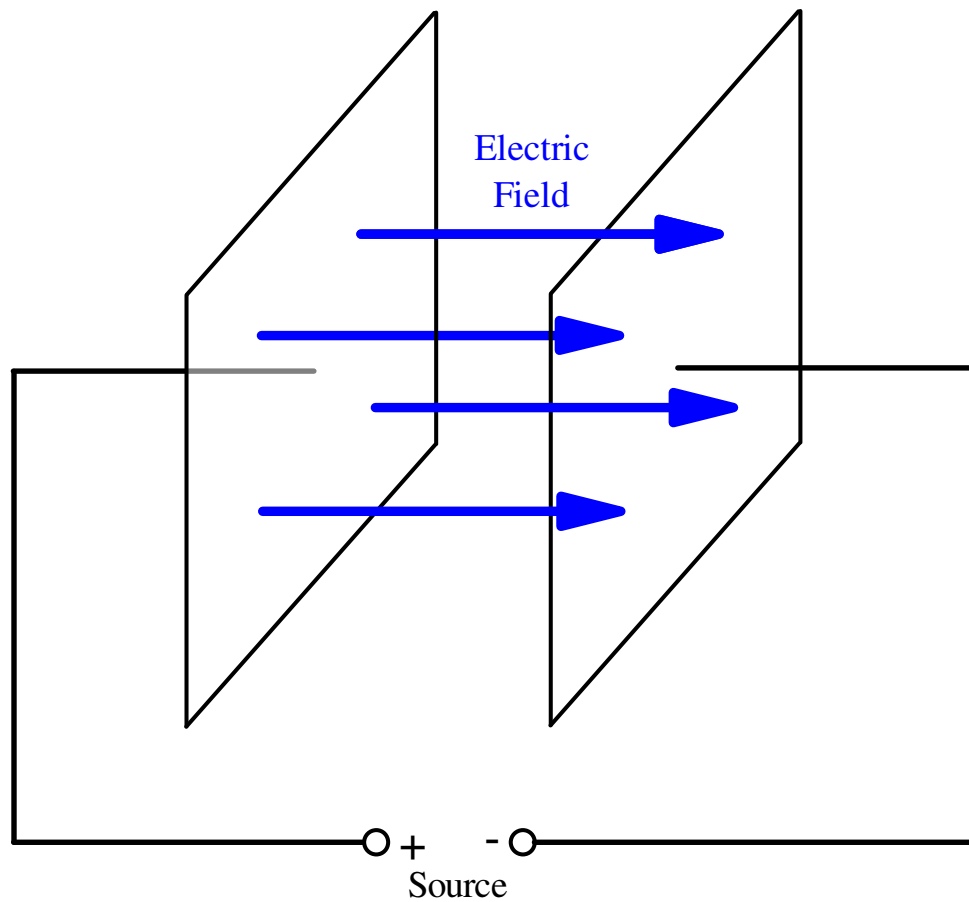


Figure 2.2: CWPT via electric field coupling between two parallel plates.

2.3 Capacitive Wireless Power Transfer Configuration

In this section, the first out of the three novel methods for capacitive wireless power transfer is introduced, as shown in Fig. 2.3. With reference to the figure, the proposed configuration consists of a pair of parallel metallic plates, one for transmitting power while another for receiving. The plates are fed by a pair of coaxial lines at the centre. It has a dimension of $L = 40\text{cm}$, $P = 24\text{cm}$, and $D = 12\text{cm}$. The variable d is the distance between the transmitting and receiving plates. An input

power of P_{in} is supplied by a 50- Ω microwave signal generator, producing uni-directional electric field between the plates. Then, the electric field is coupled by the receiving plate, with the received power being sent to a 50- Ω load. As can be seen from Fig. 2.2, electric flux is pointing from the positive-charged plate to the negative one. The ground plate functions as a return path for each of the plate.

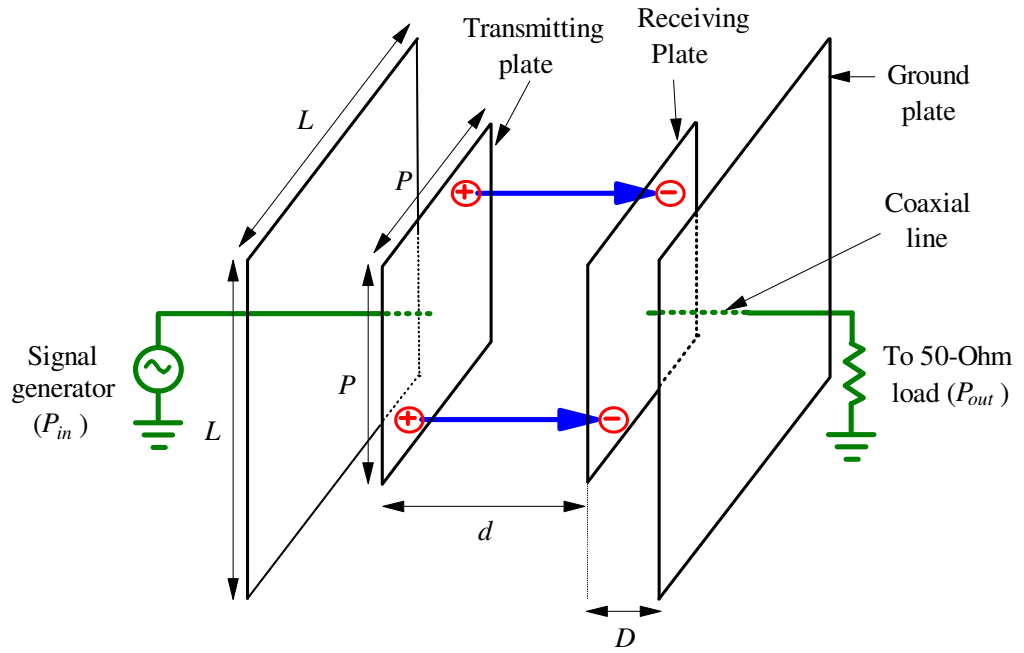


Figure 2.3: The proposed CWPT method by using a pair of parallel plates. Also shown are their respective ground plates.

For comparison purpose, an inductive wireless power transfer model is established by using a pair of coils, as shown in Fig. 2.4, working at the same operating frequency. Its performance will be compared to that for the CWPT in order to prove that the latter has better power transfer efficiency. For ease of fabrication, a pair of identical rectangular coils are designed which has a dimension of $h = 12\text{cm}$, $r = 16\text{cm}$, and $N = 4$ turns. The gap between any two neighbouring turns is always

uniform. With reference to Fig. 2.4, the transmitting coil is connected to a signal generator to supply input power P_{in} . In the similar way, one end of the receiving coil is connected to a 50- Ω load to harvest the output power P_{out} . It is the magnetic fluxes that carry the energy from the transmitting coil to the receiving load.

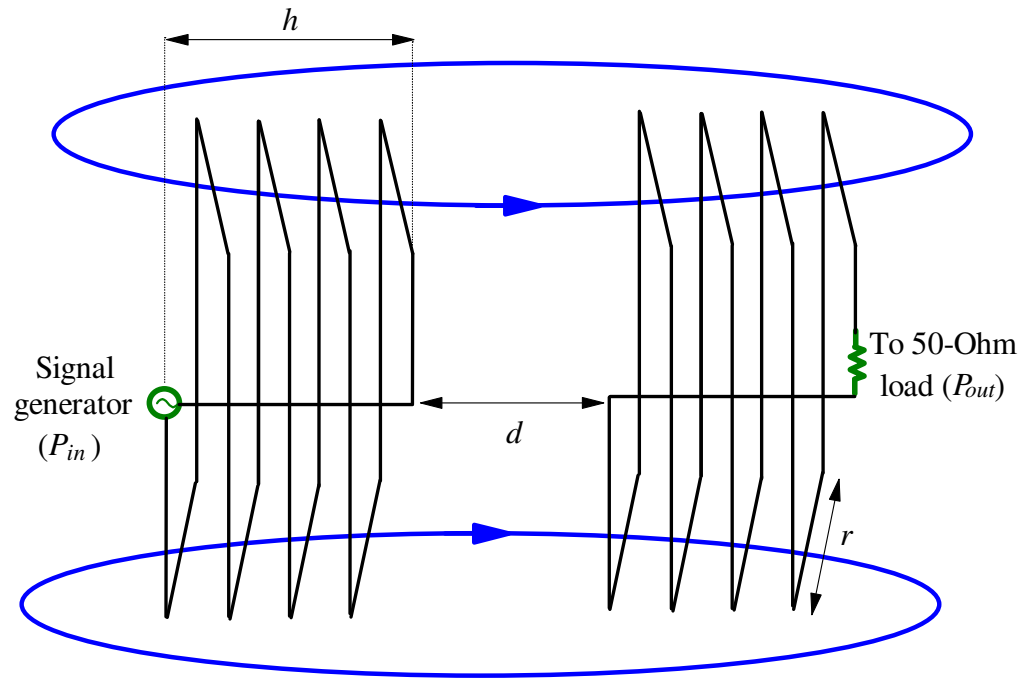


Figure 2.4: Inductive wireless power transfer demonstrated by a pair of rectangular coils. It is designed to have the same frequency as that for CWPT in Fig. 2.3.

2.3.1 Design and Optimization

The CWPT plates in Fig. 2.3 must be optimized in pair. It cannot be done separately as the plates affect each other. This is because the input impedance of the CWPT configuration is much affected by the mutual capacitance, which varies with the separation distance of the two plates. To design the plates operating at a certain

operating frequency, the two plates are first placed apart by a distance of $d = 20\text{cm}$. Then, the variables D , P , and L are adjusted so that the CWPT can achieve a maximum electric field coupling at the desired operating frequency, which is defined as the frequency point at which $|S_{21}|$ attains its maximum value ($\text{Max } |S_{21}|$) in the passband.

The conventional way to design an inductive WPT is to make the isolated coil separately. But when two coils are aligned closely, the dimension of each coil requires re-optimization as the resonant frequency shifts. Again, this is due to the change of input impedance. To have a fair comparison with the CWPT configuration, the separation distance of the coils is also designed to be $d = 20\text{cm}$. Other parameters such as r and h are then adjusted to make the coils to have the same resonant frequency as the plates.

2.3.2 Power Transfer Efficiency

The ZVB8 vector network analyzer is used for measuring the S parameters, where the maximum value of the $|S_{21}|$ ($\text{Max } |S_{21}|$) can be directly read at the operating frequency. At this frequency, an ac input power P_{in} is then supplied by a SMB100A signal generator (with 50Ω output impedance) to the transmitting plate, as can be seen from Figs. 2.3 and 2.4. The received output power (P_{out}) on the opposite plate is then measured using a FSL spectrum analyzer (with $50\text{-}\Omega$ input impedance) at the operating frequency. The measured power transfer efficiency (PTE) can then be calculated as $\text{PTE} = (P_{out} / P_{in}) \times 100\%$. On the other hand, the simulated PTE =

$|S_{21}|^2 \times 100\%$ is directly obtained from the simulated maximum $|S_{21}|$, where $|S_{21}|$ is in linear scale. The calculation methods will be applied throughout the dissertation.

2.4 Results and Discussions

In this section, the proposed CWPT and coil configurations were simulated by using the CST Microwave Studio software. The coupling coefficient, reflection coefficient, and input impedance of the fabricated prototypes were measured on a ZVB8 vector network analyzer.

2.4.1 Separation Distance

Fig. 2.5 compares the operating frequency, maximum $|S_{21}|$, as well as the impedance matching of the CWPT (Fig. 2.3) and coupling coils (Fig. 2.4). As both of the power transfer systems are symmetrical, the reflection coefficients $|S_{11}|$ and $|S_{22}|$ are expected to be identical at the input and output ports. Here, only $|S_{11}|$ is shown. With reference to Fig. 2.5(a), it can be clearly seen that both the measured and simulated maximum $|S_{21}|$ of the coils drop at a much rapid rate with distance d , faster than for the CWPT. It reflects that the coupling efficiency of the coils deteriorates faster than that of the parallel plates (CWPT) as d increases. This is not surprising as more magnetic fields are leaked for a larger d . As can be seen from the figure, the maximum $|S_{21}|$ of the CWPT is higher than the coils over the entire measurement range 0.5cm - 20cm. Except for CWPT at $d = 0.5\text{cm}$, the measured and simulated

operating frequency of the plates and coils are well confined within 110 to 130MHz. With reference to Fig. 2.5(b), for $d \leq 8\text{cm}$, measurement results show that $|S_{11}|$ of the CWPT is better than that of coils at the operating frequency. It implies that the CWPT configuration possesses a better input impedance matching condition than the coils. This is potentially caused by the input reactance or inductance of the coils being higher than the input reactance or capacitance of the CWPT in this range, which in turn results in the coils having larger input impedance mismatch with the $50\text{-}\Omega$ source. Larger mutual inductance (L) between the coils for nearer distance, d causes larger input reactance of the coils, which is $X_L = 2\pi fL$. However, larger mutual capacitance (C) between the plates in the CWPT results in the input reactance of the CWPT gets smaller, which is $X_C = 1/(2\pi fC)$.

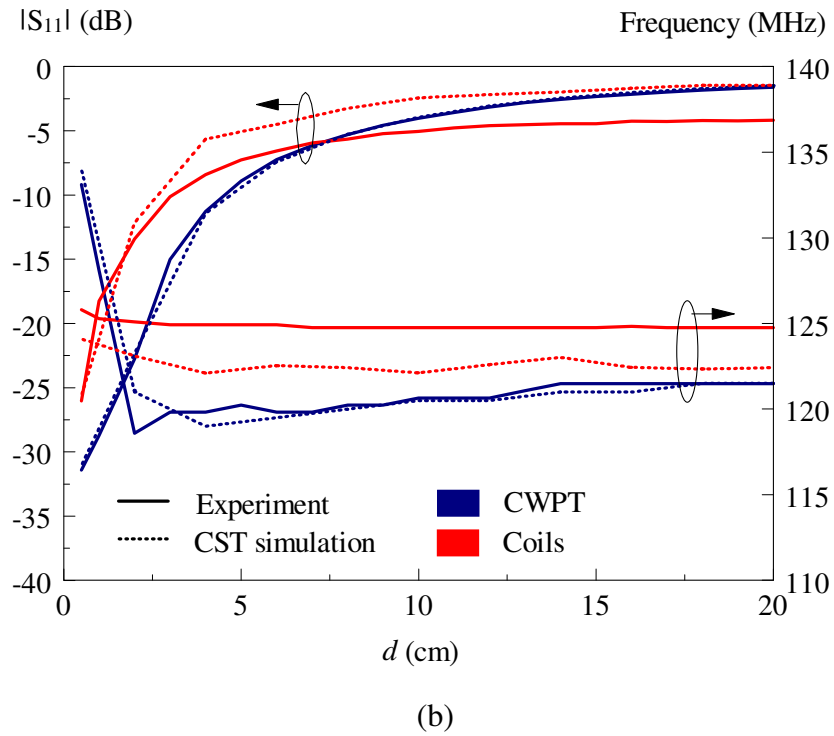
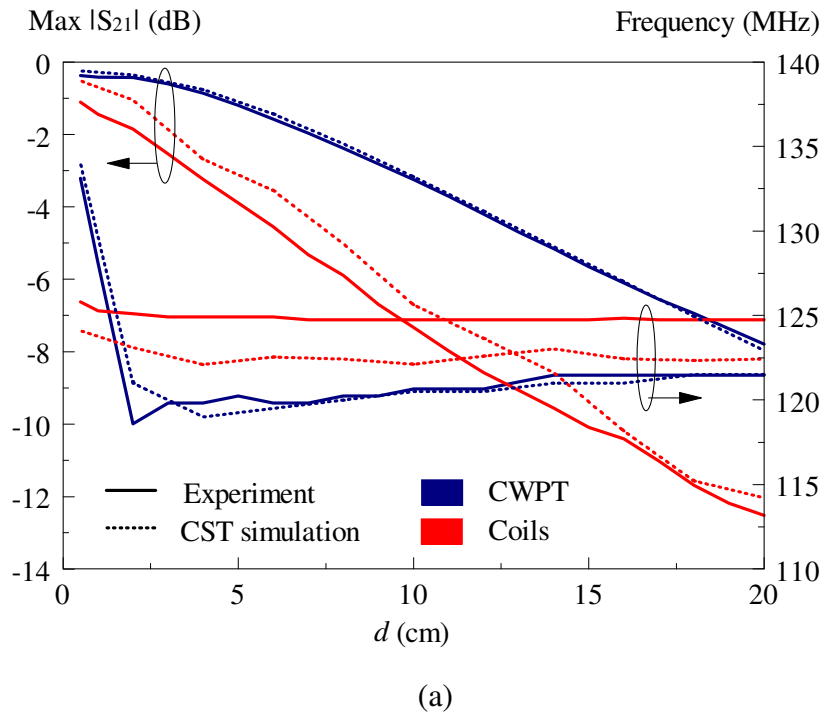


Figure 2.5: Comparison of the performances of the plates and coils: (a) Maximum coupling coefficient. (b) Reflection coefficient $|S_{11}|$ at Max $|S_{21}|$. The respective operating frequencies are also shown in the figures.

The PTE of the CWPT and coils are measured by a SMB100A signal generator and a FSL spectrum analyzer. Fig. 2.6 compares the measured and simulated PTE of the CWPT and coils at their respective operating frequencies (obtained in Fig. 2.5). It can be seen that the PTE of CWPT is higher than that of the coils over the entire measurement range. This is not surprising as higher $|S_{21}|$ implies a higher PTE. At $d = 20\text{cm}$, the measured PTE of the CWPT and coils are 16.63% and 3.86% respectively, with a difference of 12.77%. At $d = 0.5\text{cm}$, the measured PTE of the CWPT is 91.78%, which is 10.12% higher than for coils of 81.66%.

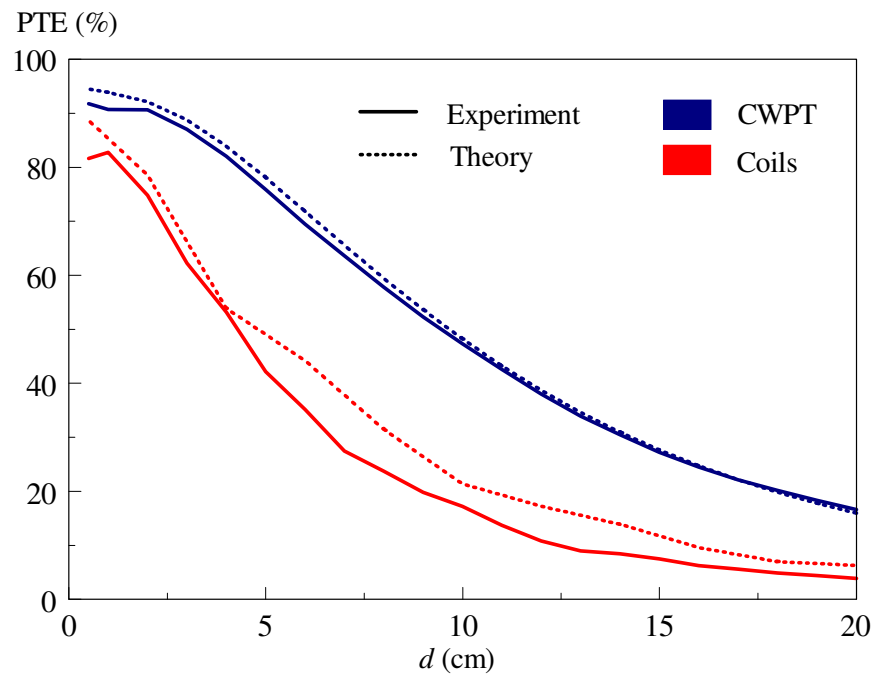
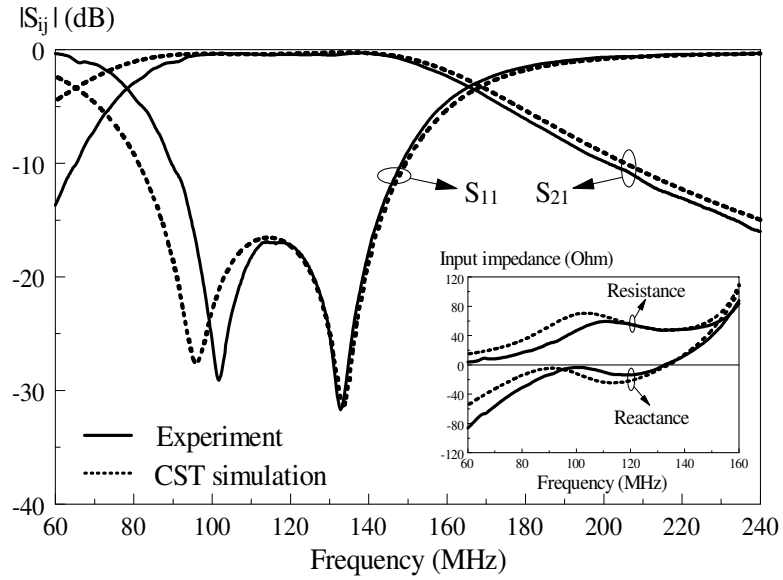


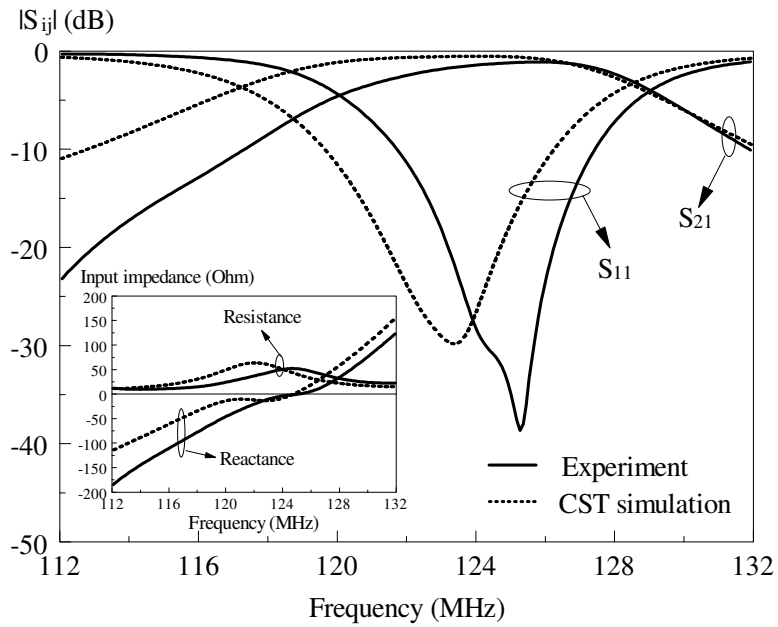
Figure 2.6: Comparison of the PTE for the CWPT and coils.

Next, the efficiency of the two WPT configurations with very small separation distance $d = 0.5\text{cm}$ will be discussed. Fig. 2.7 (a) and (b) show the measured and

simulated S parameters of the CWPT and coils at $d = 0.5\text{cm}$. Their corresponding input impedances are depicted in the insets.



(a)



(b)

Figure 2.7: The measured and simulated S parameters and input impedance at $d = 0.5\text{cm}$: (a) CWPT. (b) Coils.

The performance of the CWPT at $d = 0.5\text{cm}$ will first be discussed. With reference to Fig. 2.7(a), the measured and simulated operating frequencies of the CWPT at $d = 0.5\text{cm}$ are 133.12MHz and 134MHz, respectively, with an error of 0.66%. At the operating frequencies, the measured maximum $|S_{21}|$ is -0.3727dB, which is 0.127dB lower than the simulated $|S_{21}|$ of -0.2457dB. As can be found in Fig. 2.6, the measured PTE at $d = 0.5\text{cm}$ is 91.78%, which is slightly lower than the simulated PTE of 94.5%. At $d = 0.5\text{cm}$, the measured and simulated input impedances are $47.6 + j1.03\Omega$ and $47.69 + j0.34\Omega$ respectively, which are very close to the source impedance of 50Ω . The CWPT configuration has a good input impedance matching for small d , which in turn is capable of providing high PTE.

Now, the performance of the coils will be discussed. Referring to Fig. 2.7(b), the measured operating frequency of the coils at $d = 0.5\text{cm}$ is 125.8MHz, which is slightly higher than the simulated one of 124.1MHz (with an error of 1.37%). At these frequencies, the measured $|S_{21}|$ is -1.101dB, which is 0.585dB lower than the simulated one of -0.516dB. In Fig. 2.6, it has been shown that the measured and simulated PTEs are 81.66% and 88.71% respectively, with a difference of 7.05%. The measured and simulated input impedances are $48.02 + j3.82\Omega$ and $49.48 - j7.24\Omega$ at the respective operating frequencies. Again, an impedance of nearly 50Ω and a high value in PTE show that the coils have been optimized for this distance d . However, the PTE of coils is lower than that for the CWPT as plates can confine the uni-directional electric field better.

Another advantage of the CWPT over the coils is its wide bandwidth. The measured and simulated bandwidths ($|S_{21}| > -3\text{dB}$) of the CWPT (Fig. 2.7(a)) are

69.13% and 85.47% respectively. Meanwhile, the measured and simulated bandwidths of the coils are 5.6% and 8.47%. It is interesting to note that the bandwidth of the CWPT configuration is ~ 60 - 80% wider than the coils.

2.4.2 Parametric Analysis for CWPT

Two groups of simulations will be performed to study the characteristics of the CWPT. Firstly, by keeping $d = 10\text{cm}$, the distance D of the transmitting and receiving plates is varied from 1 to 50cm from their respective ground plates. The simulated operating frequencies and maximum $|S_{21}|$ are shown in Fig. 2.8. With reference to the figure, a sharp increase in operating frequency is observed when D is increased from 1cm to 4cm. Then, it is decreasing slowly with increasing D until 50cm. Weak coupling at $D = 1\text{cm}$ is due to the cancellation of the induced charge on plate with its image on the ground, which are opposite in polarity. This happens only when the plate comes too close to the ground.

Increasing D from 1cm to 10cm (with $d = 10\text{cm}$), as can be seen in Fig. 2.8, a surge in the maximum $|S_{21}|$ is observed. This is because the capacitance effect between the plate and ground can be significant if D is small enough. A metallic plate has the tendency to form strong electric fluxes with the metal nearest to it. Beyond $D = 10\text{cm}$, $|S_{21}|$ increases slowly.

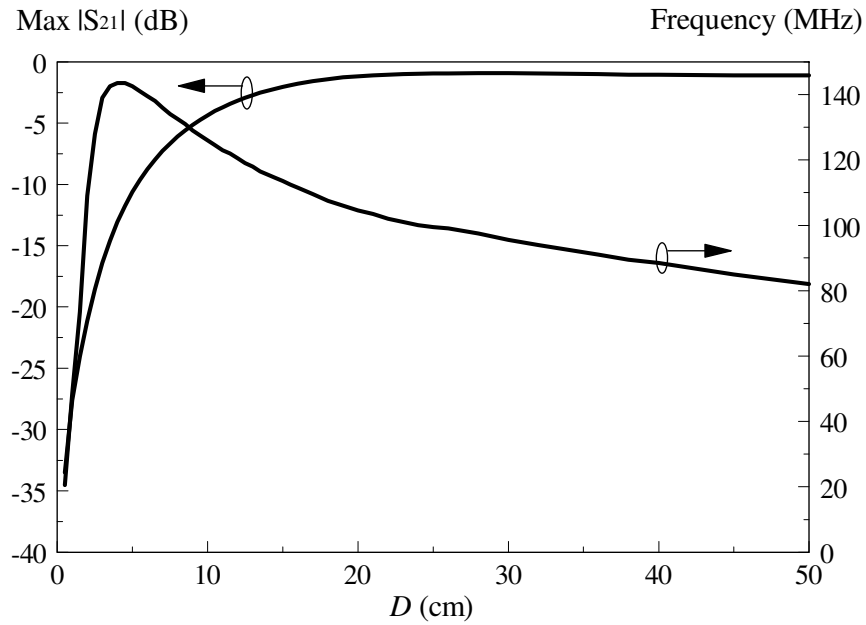


Figure 2.8: Operating frequency and the corresponding maximum $|S_{21}|$ of the CWPT as a function of the plate-to-ground distance D .

Another group of simulations performed shows that the coils exhibit the similar behaviour. By varying the height of coils h while maintaining the radii and number of turns, the changes in the operating frequency and the corresponding maximum $|S_{21}|$ are shown in Fig. 2.9. In all cases, the distance between the coils d is always fixed at $d = 10\text{cm}$. The $|S_{21}|$ was found to be improving monotonously with h . The change of the h from 6 to 18cm improves the $|S_{21}|$ drastically from -13.563dB to -3.804dB, implying a significant enhancement of PTE. It can be noted that the operating frequency only changes slightly with h .

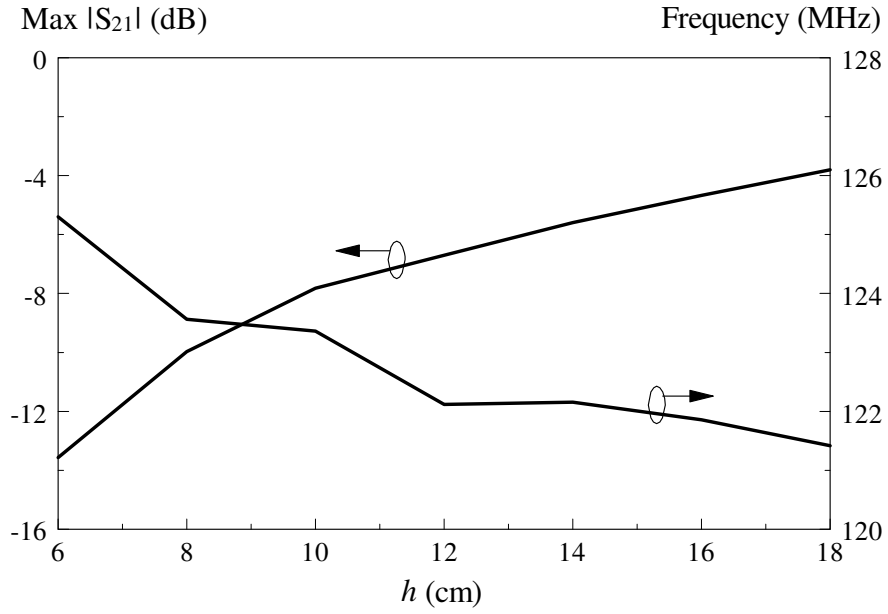


Figure 2.9: Operating frequency and the corresponding maximum $|S_{21}|$ of the coils as a function of the coil height h , with $d = 10$ cm.

Comparing the results shown in Fig. 2.8 and 2.9, it is clear that the PTE of the CWPT and coils can be further improved by increasing the D and h , respectively. However, in order to have a fair PTE comparison and a compromise between the size and PTE of the WPT models, both the D and h are fixed to a same value of 12cm.

Next, by keeping $d = 10$ cm and $D = 12$ cm in the CWPT configuration, the effect of the ground size on the operating frequency and maximum $|S_{21}|$ is studied. The result is shown in Fig. 2.10. With reference to the figure, the maximum $|S_{21}|$ increases monotonously with the increase of the ground. From $L = 5$ cm to 40cm, the maximum $|S_{21}|$ increases at a much faster rate than in 40 - 100cm. This shows that the ground size has to be designed large enough ($L \geq 40$ cm). Beyond $L = 40$ cm, although the increase rate is slow, the value of maximum $|S_{21}|$ is still going up with L .

This is due to the enhancement of field-confining capability of the larger ground plates which enables better electric field coupling between the plates. Below $L = 30\text{cm}$, the operating frequency is found to be decreasing drastically. Again, this is caused by the strong interaction of the charges on plate and their image charges on ground. Beyond $L = 30\text{cm}$, the operating frequency becomes more consistent. Larger ground size causes the power transfer to improve without affecting the operating frequency much. But it increases the system size.

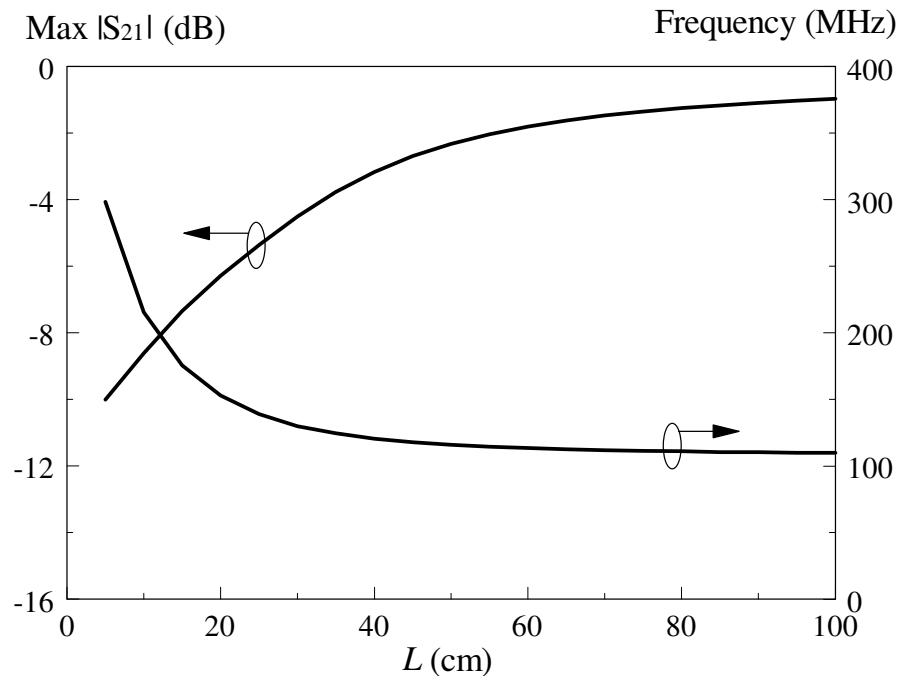


Figure 2.10: Operating frequency and the corresponding maximum $|S_{21}|$ of the CWPT as a function of ground size L .

2.4.3 2×2 Array for CWPT

In this section, simulations are performed where four plates are designed into 2×2 array form using the same CWPT configuration depicted in Fig. 2.3, with the

new structure given in Fig. 2.11. Referring to the figure, all the transmitting plates are sharing a common ground plate. This holds for the receiving side as well. The electric fields used for power transfer are well confined within each pair of parallel plates, without much interference with the fields from other plates. Therefore, the transmission coefficient $|S_{21}|$ of each plate remains basically unchanged. Due to this reason, the total received current (I_a) will be used as the parameter to describe the performance of CWPT array. In this case, 1W of power is supplied to each of the input port. All the port impedances are predefined to be 50- Ω . By exciting the four input ports simultaneously, the total current at the array output is the sum of currents at all ports.

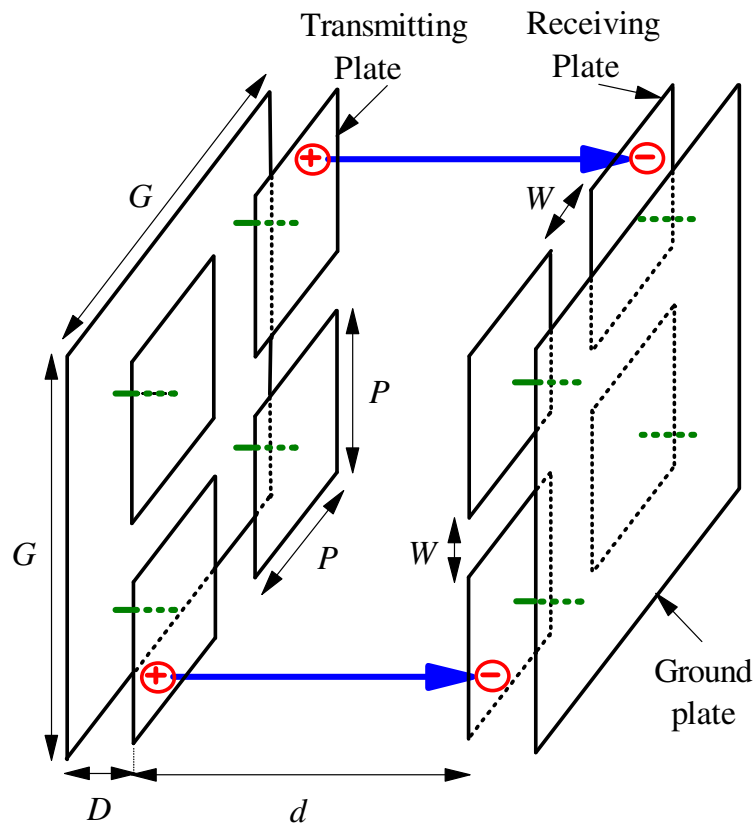


Figure 2.11: A 2×2 array for the CWPT.

First, the change of the total received current I_a with the separation distance d is investigated. The CWPT array has a dimension of $D = 12\text{cm}$, $P = 24\text{cm}$, $W = 20\text{cm}$, and $G = 84\text{cm}$. Fig. 2.12 shows the simulated I_a together with the corresponding operating frequency. Also given is the received current (I_s) for a single pair of parallel plates (Fig. 2.3), with the same power (1W) supplied to the input port. Ideally, I_a should be four times of I_s . But it can be seen from the figure that the value of I_a is not exactly four times of I_s . The ratio of I_a to I_s is around 3.4 to 4.3. This ratio is obtained by dividing the magnitude of I_a by the corresponding magnitude of I_s for each value of d , respectively. The loss can be caused by the cross coupling between the plates. At certain distance d and operating frequency, constructive interferences may take place in between the fringing fields from the plates, which contribute to additional current at each of the output port. This additional interference-generated current could cause the current received by each of the output port being larger than the case of single element, I_s . Therefore, the ratio of I_a to I_s being larger than 4 is possible for this configuration.

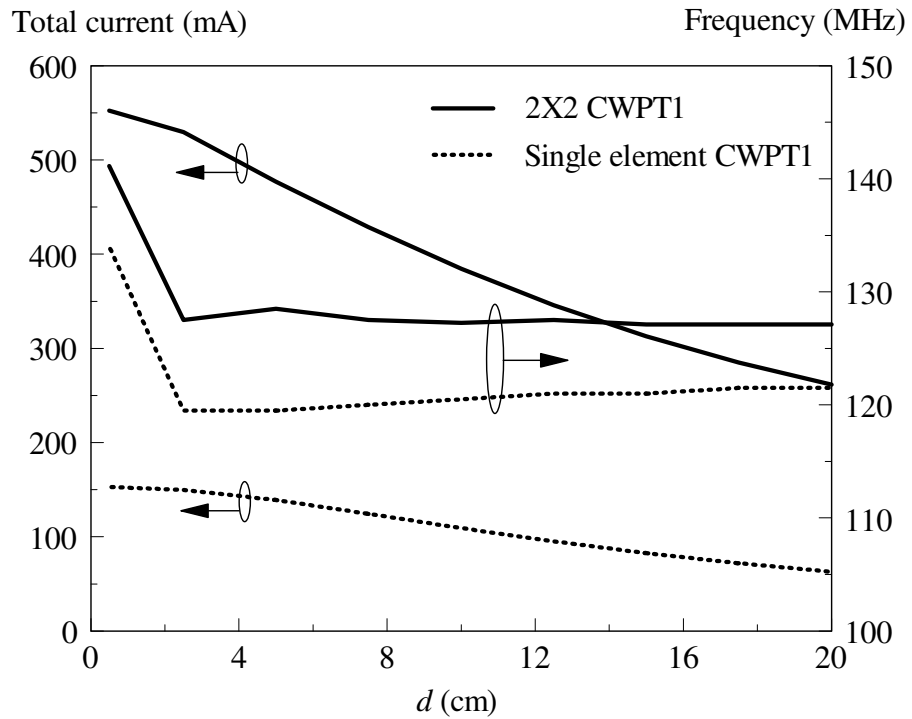


Figure 2.12: Total received current (I_a) and operating frequency of the 2×2 CWPT as a function of d . Also given is the current of the single-plate (I_s).

In the next group of simulations, the effect of the separating distance between the plates W is investigated. The dimension of the model is designed to be $d = 10\text{cm}$, $D = 12\text{cm}$, and $P = 24\text{cm}$. It can be observed from Fig. 2.13 that the simulated total received current I_a and the corresponding operating frequency are affected by W .

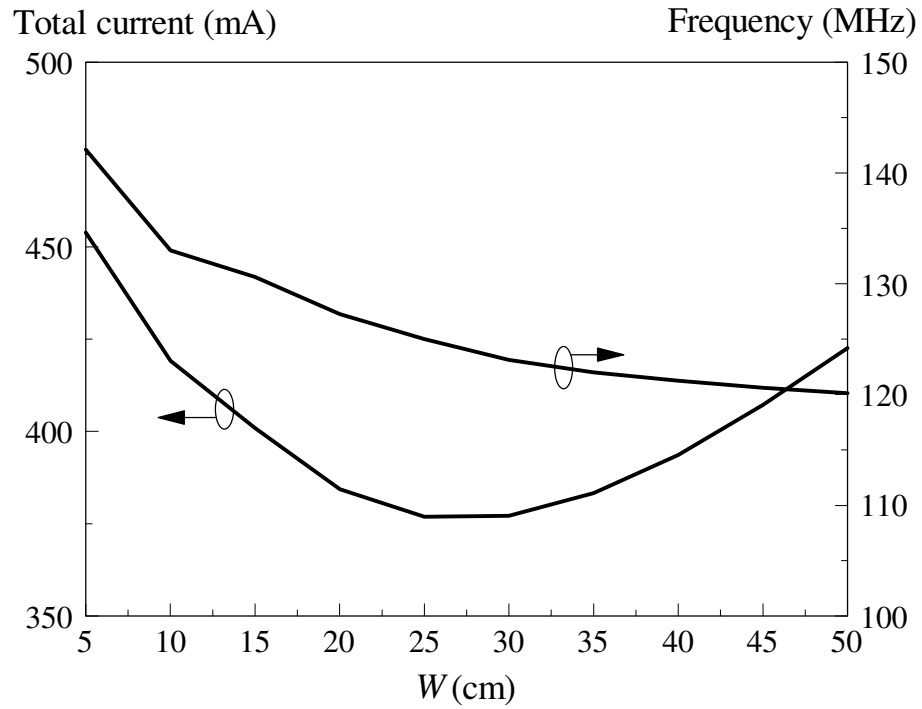


Figure 2.13: Total received current as a function of W . Also given is its corresponding operating frequency.

2.5 Conclusion

A novel method for CWPT by using a pair of parallel plates has been presented. The proposed CWPT configuration is able to transfer wireless power more efficiently than coils at the same operating frequency. Simultaneous power transfer of the 2×2 CWPT array has also been investigated. The use of parallel plates for transmitting wireless power can be a possible solution to power up the complex electronic systems in the future.

CHAPTER 3

WIRELESS POWER TRANSFER FOR MOTHERBOARD PERIPHERALS

3.1 Introduction

This chapter explores a new way for transferring wireless power to the electronic components and integrated circuits (IC) in a computer motherboard. Fig. 3.1 is a photograph showing the peripheral PCBs which are vertically inserted into the PCI slots of a motherboard for data communication, as well as to supply electric power. This is a well-known standard protocol working for years. In order to supply electricity to thousands of chips and integrated circuits (IC) on the computer peripherals, the wire routes and traces can get very complex. Such configuration is not only occupying large footprint, also, it has poor electromagnetic compatibility performance.

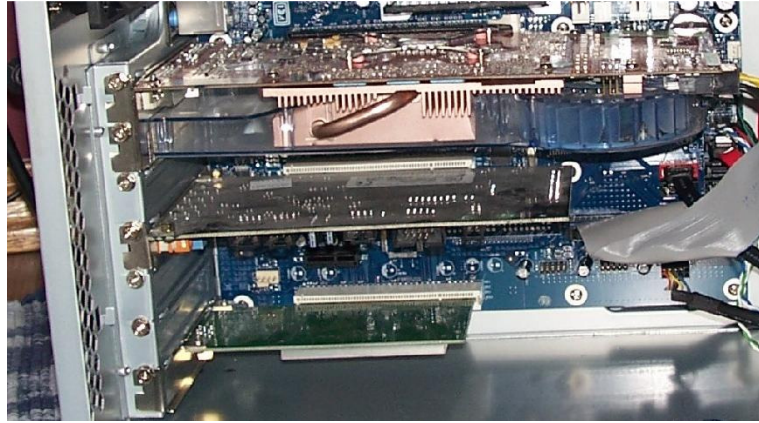


Figure 3.1: Peripheral printed circuit boards inside a computer casing.

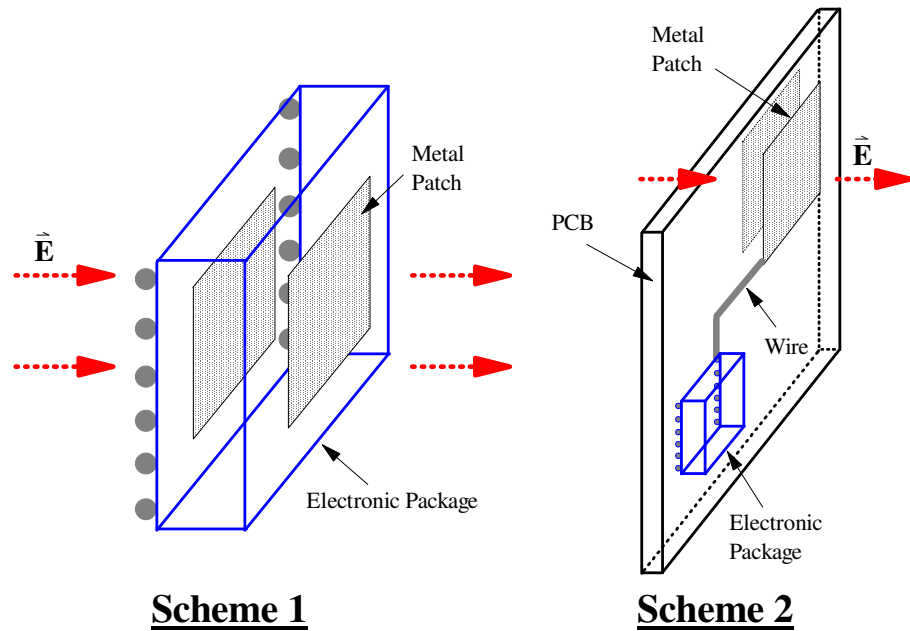


Figure 3.2: The proposed power transfer schemes for chips and ICs on the peripheral boards.

For the first time in this dissertation, a convenient way to transfer wireless power to the computer peripherals is introduced using the two proposed schemes illustrated Fig. 3.2. In the first case, two metal patches are deposited on the top and bottom surfaces of an electronic package to harvest electric power. Alternatively, as

illustrated in Scheme 2, the pair of patches can be directly deposited onto the PCB substrate to channel power to an IC chip. By such, long wires that are necessary to connect the chip to the motherboard can be avoided. A wireless powering setup, imitating the proposed models in Fig. 3.2, will then be established to verify the proposed ideas, along with the discussion of the detailed working principles in *Section 3.2*. As electric field is exploited, the corresponding capacitive effect will be elucidated. In *Section 3.3*, experiment is conducted to verify the simulation models.

3.2 Model Configuration

With reference to Fig. 3.3, two larger plates ($L_1 \times L_1$) are connected to a 50- Ω signal source with an internal impedance of Z_o to supply electric power. The receiving plates ($L_2 \times L_2$), which are embedded inside the larger ones, are used to channel the harvested power to an output load ($Z_L = 50\Omega$). Capacitors C_1 and C_2 are for matching the input and output impedances. Two different cases will be explored here. In the first, two pairs of parallel plates ($L_1 = L_2 = 15\text{cm}$) of equal size are considered a maximum coupling. The two internal plates are separated with a small gap of $D = 5\text{mm}$, imitating the package or PCB thickness. The second case is to study the power transfer from two larger plates ($L_1 = 15\text{cm}$) to the smaller. A pair of plates ($L_2 = 7.5\text{cm}$) with quarter of the size of the larger ones are used. Here, input power is given to the outer plates and received by the inner ones. The distance between the internal and external plates d will then be varied for the power transfer measurements. Although only one is demonstrated, the internal region can actually accommodate more than one pair of patches. In experiment, the external plates are

connected to a microwave signal generator R&S SMB 100A with $Z_o = 50\Omega$ through two short copper wires (diameter $\sim 1\text{mm}$). At the power receiving end, the same type of copper wires are used to connect the inner plates to a microwave spectrum analyzer having a $50\text{-}\Omega$ internal impedance which in turn functions as the load Z_L . The connection between the external plates and the signal generator is made by first soldering a copper wire to each of the plate. These two wires are then connected to a SMA female connector, with one soldered to the centre core of the connector and the other soldered to its braid. The connection between this SMA female connector and SMA female output connector of the signal generator can be completed through a SMA male-to-male cable. The same method is applied to the connection between the internal plates and the spectrum analyzer. The capacitors C_1 and C_2 that are connected across the signal generator and output load are used to transform both the input and output impedances to 50Ω simultaneously so that it can match to the internal impedances of the signal generator and spectrum analyzer without needing any additional impedance matching circuits. Different C_1 and C_2 values are used when the plates' separation distance d is varied as the input and output impedances are changing.

In this chapter, both simulations and experiments will be carried out to study the operating frequency and the power transfer efficiency (PTE) of the proposed power transfer schemes for different values of d . The operating frequency can be determined by taking the frequency point at which $|S_{21}|$ reaches maximum reading, either in simulation or experiment. To calculate the simulated PTE at the operating frequency, the transmission coefficient $|S_{21}|$ obtained from the CST simulation is directly plugged into the theoretical definition of $|S_{21}|^2 \times 100\%$. On the other hand,

the experimental power transfer efficiency (PTE) can be calculated by P_{out} / P_{in} , where the input power (P_{in}) and output power (P_{out}) are directly read from the signal generator and spectrum analyzer, respectively, at the operating frequency. The frequency tracking function of the spectrum analyzer has been used for a more accurate reading.

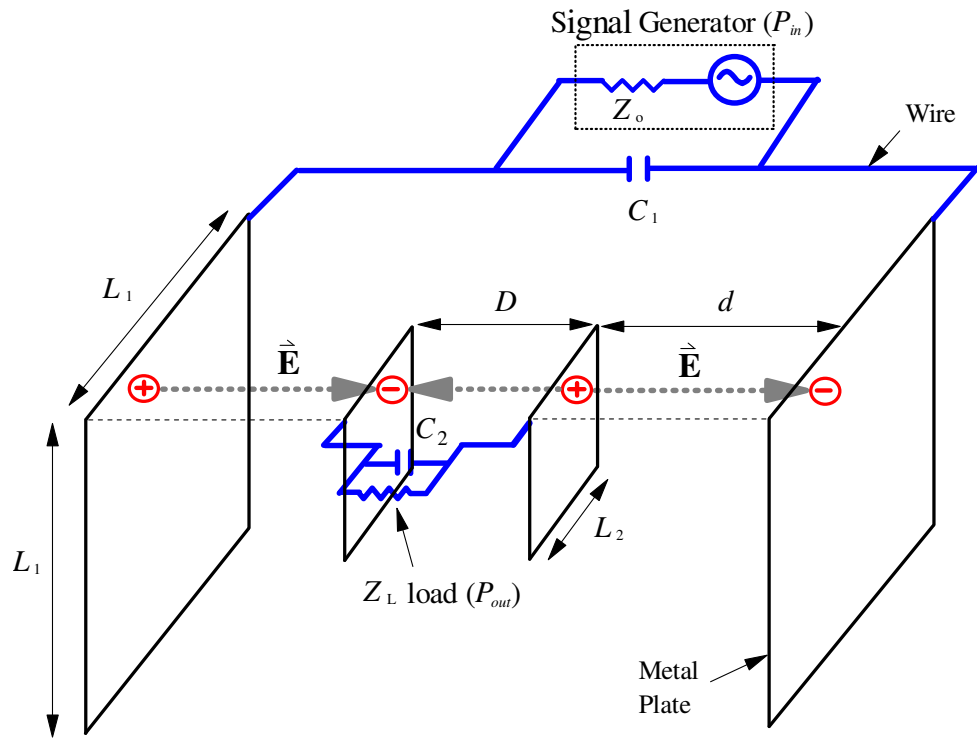


Figure 3.3: Experiment setup for demonstrating the proposed power transfer schemes for chips and ICs.

3.2.1 Electric Field Mechanism

The electric field mechanism of power transfer is now studied. Assuming that one pair of charges are induced on the external plates at a certain snapshot, as can be seen from Fig. 3.3, another equal pair of opposite charges will then be attracted to the

adjacent internal plates. The direction of the electric field that is formed by the charges on the internal plates is exactly opposite to that of the external ones. Formation of the electric fields enables the exchange of energy from the external plates to the internal. At the end, the energy collected by the internal plates is delivered to the output load Z_L . It can also be seen from Fig. 3.3 that the internal plates, which are totally embedded inside the two larger or equal plates, are forming a closed loop together with the loading resistors and capacitors to enable current flow. Obviously, the energy amount that is coupled to the internal plates is linearly proportional to the plate size and input power P_{in} . Larger plate area enables more fluxes to reach the internal plates. The PTE is mainly dependent on the distance between the power transmitting and receiving plates, d . Simulations and the corresponding experiments will be carried out to verify it.

3.2.2 Impedance Matching

Other than the distance between the plates, another most critical parameter that determines the PTE is the impedance matching condition at the input and output ports. With reference to Fig. 3.4(a), it will be shown that the proposed parallel plates system has inherent low resistance at both the input port $\text{Re}\{Z_{in}\} = R_{in}$ and output port $\text{Re}\{Z_{out}\} = R_{out}$, making it difficult to match with other wireless systems, which usually have an impedance of 50Ω . With the use of a pair of matching capacitors C_1 and C_2 , as can be seen in Fig. 3.4(b), the impedances at both ports can be raised such that $Z'_{in} \sim 50\Omega$ and $Z'_{out} \sim 50\Omega$. In experiment, however, achieving exact impedance matching is extremely difficult as capacitors are only available in certain discrete

values. Effort has been made to make the real part of the input and output impedances as close as possible to 50Ω , with a minimum reactance.

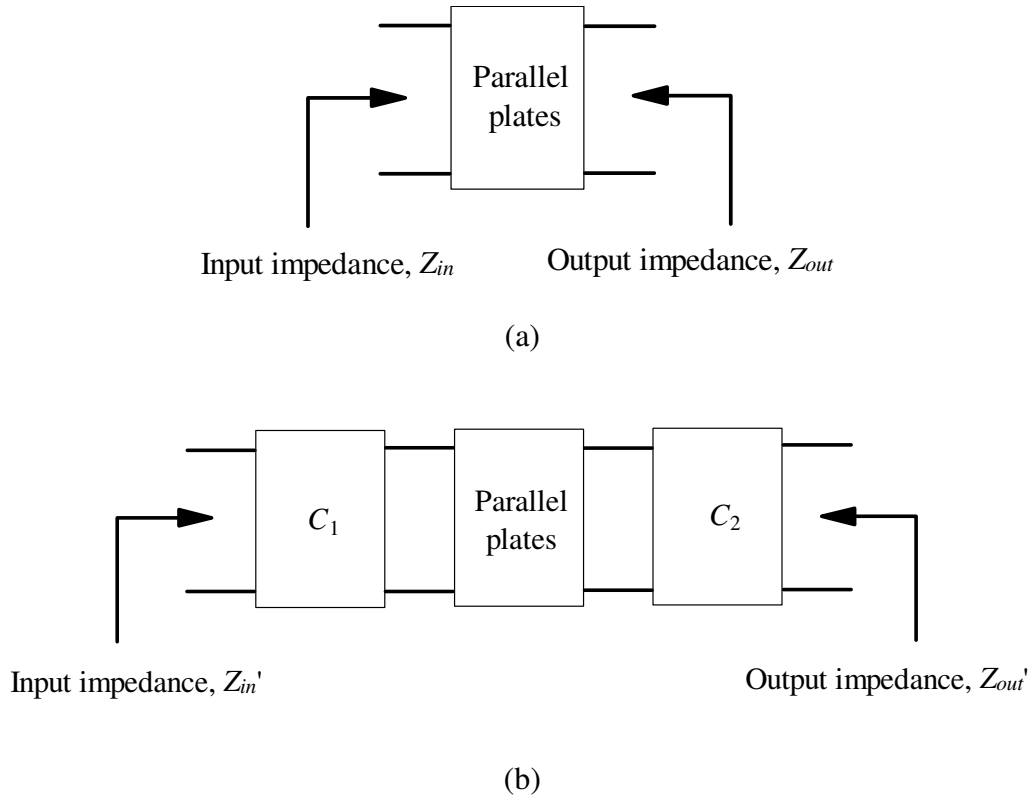


Figure 3.4: The network model of the proposed parallel plates system: (a) Without matching capacitor. (b) With matching capacitors.

3.3 Results and Discussion

The proposed new power transfer scheme is simulated using the CST Microwave Studio. Measurements of S-parameter are done by using the ZVB8 vector network analyzer. The PTEs are measured by a SMB100A signal generator and a FSL spectrum analyzer.

Two pairs of equal parallel plates are studied first ($L_1 = L_2 = 15\text{cm}$). Fig. 3.5 shows the simulated and measured S parameters of the configuration at $d = 0.5\text{cm}$ and $D = 0.5\text{cm}$. The optimum matching capacitors are $C_1 = 39\text{pF}$ and $C_2 = 47\text{pF}$. With reference to the figure, the measured $|S_{21}|$, $|S_{11}|$, and $|S_{22}|$ agree well with their respective simulated counterparts. The measured and simulated operating frequencies (at maximum $|S_{21}|$) are 196.25MHz and 197.4MHz respectively, with an error of 0.58% . At the operating frequency, the measured maximum $|S_{21}|$ is -0.345dB , which is slightly lower than the simulation of -0.145dB . From the definition of $|S_{21}|^2 \times 100\%$, the simulated PTE is calculated to be 96.72% . With the use of signal generator and spectrum analyzer, the measured PTE yields 91.42% at the operating frequency of 196.25MHz , being slightly lower than its simulation.

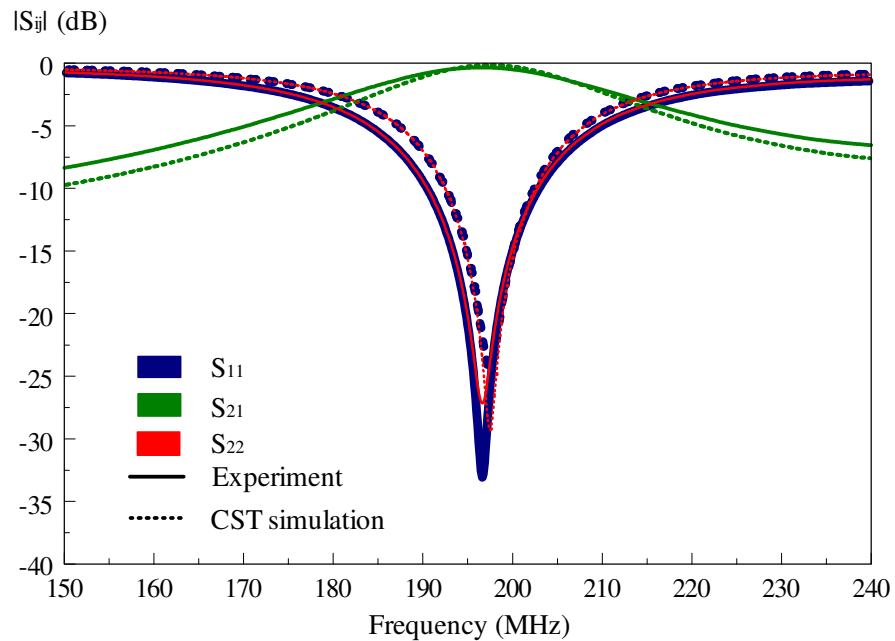
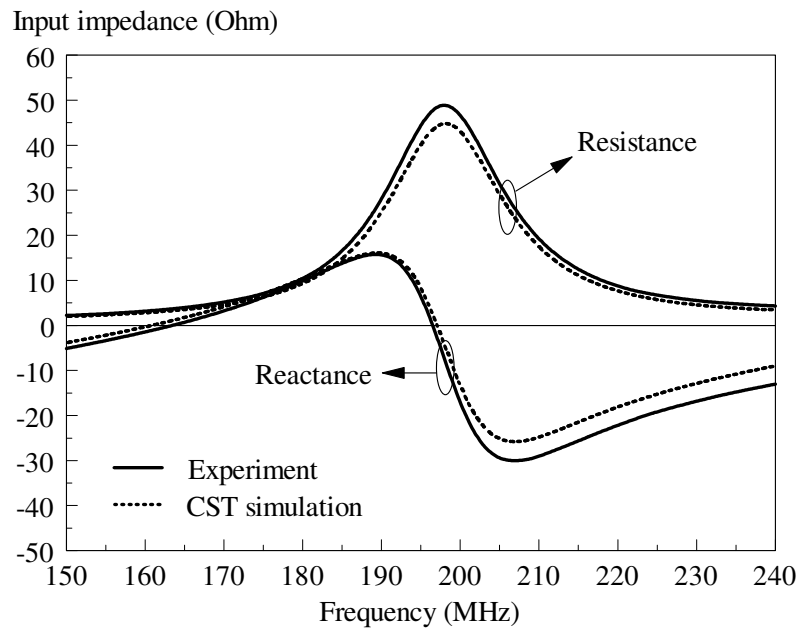
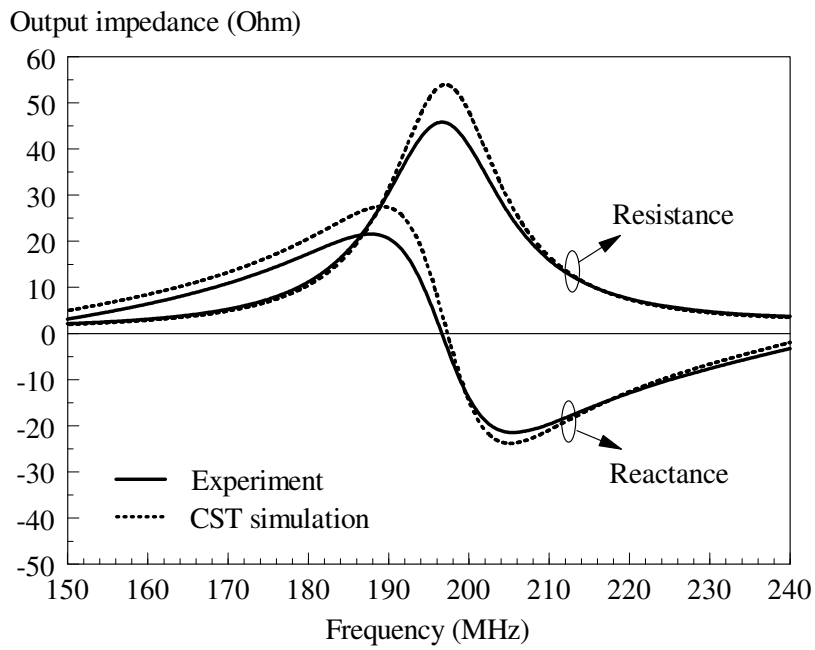


Figure 3.5: Measured and simulated S parameters for the equal plates ($L_1 = L_2 = 15\text{cm}$) at $d = 0.5\text{cm}$ and $D = 0.5\text{cm}$.

For the $L_1 = L_2$ case, the measured and simulated input and output impedances at $d = 0.5\text{cm}$ and $D = 0.5\text{cm}$ are shown in Fig. 3.6(a) and (b), respectively. Referring to Fig. 3.6(a), both the measured input resistance and reactance agree well with their simulated counterparts. Here, the measured input impedance at the operating frequency (196.25MHz) is $47.28 + j1.23\Omega$, which is very close to the simulated one of $44.54 - j1.54\Omega$ (at 197.4MHz). With reference to Fig. 3.6(b), the corresponding measured and simulated output impedances are $45.72 + j1.77\Omega$ and $53.84 - j0.56\Omega$, respectively. The slight discrepancy between the measured and simulated input and output impedances can be caused by component tolerance of the capacitors.



(a)



(b)

Figure 3.6: Measured and simulated impedances of the equal plates at $d = 0.5\text{cm}$ and $D = 0.5\text{cm}$: (a) Input impedance. (b) Output impedance.

Next, the PTE is studied for different separation distances (d) between the plates. Table 3.1 shows the measured and simulated operating frequencies (at maximum $|S_{21}|$) and their corresponding $|S_{21}|$ for d of 0.5cm, 1cm, and 1.5cm. In all cases, the distance between the internal plates is always kept at $D = 0.5$ cm. Also appended are the measured and simulated PTEs. The corresponding capacitance values C_1 and C_2 for all d distances are tabulated in Table 3.2. With reference to Table 3.1, the measured maximum $|S_{21}|$ at $d = 0.5$ cm, 1cm, and 1.5cm are -0.3448dB, -0.5387dB, and -1.0388dB respectively, which are slightly lower than their respective simulated counterparts of -0.1453dB, -0.3476dB, and -0.4764dB. It can be seen that the operating frequencies in all cases fall within the frequency range of 190MHz - 220MHz. In Table 3.1, the simulated PTE is calculated based on the simulated $|S_{21}|$ given in the same table using the definition $\text{PTE} = |S_{21}|^2 \times 100\%$ for different values of d . The simulated and measured PTEs agree well with each other, seeing both of them decrease with d . As can be seen from the table, the measured PTE reduces from 91.41% to 86.3% as the plates separation is increased from 0.5cm to 1.5cm. Meanwhile, the simulated PTE reads 96.71% at $d = 0.5$ cm and 89.61% at $d = 1.5$ cm, which are 5.3% and 3.31% higher than their respective measured counterparts. The results are expected due to the decrease in electric field intensity between the plates as d increases, causing less energy to be transferred from the outer to the inner plates.

Table 3.1: Measured and simulated $|S_{21}|$, PTE, and operating frequencies of the equal plates configuration ($L_1 = L_2 = 15\text{cm}$) at different d values.

d (cm)	Insertion Loss, Max($ S_{21} $), (dB)		PTE (%)		Operating Frequency (MHz)	
	CST Sim.	Exp.	Theory	Exp.	CST Sim.	Exp.
0.5	-0.1453	-0.3448	96.71	91.41	197.4	196.25
1	-0.3476	-0.5387	92.31	90.99	214.2	215.50
1.5	-0.4764	-1.0388	89.61	86.30	197.8	200.25

Table 3.2: Capacitances used for different values of d for the equal parallel plates configuration ($L_1 = L_2 = 15\text{cm}$).

d (cm)	C_1 (pF)	C_2 (pF)
0.5	39	47
1	39	27
1.5	39	68

Now, the effects of the matching capacitors at the input and output are discussed. The input and output impedances of the configuration shown in Fig. 3.3 are studied for the cases with and without matching capacitors at the plates separation of $d = 0.5\text{cm}$, 1cm , and 1.5cm , with the corresponding measured and simulated resistances and reactances being compared in Table 3.3 (a) and (b). With reference to Table 3.3 (a), it can be seen that the input resistances of the parallel plates without the matching capacitors are small in general for all values of d . Here, the measured resistances read 5.39Ω , 3.88Ω , and 3.65Ω at the distances of $d = 0.5\text{cm}$,

1cm, and 1.5cm, respectively, agreeing well with the simulated ones of 4.84Ω , 3.51Ω , and 3.4Ω . This causes inconvenience as it is difficult to match the plates with other $50\text{-}\Omega$ communication systems. By including capacitors C_1 and C_2 to the input and output ports, the new resistances are measured as 47.28Ω , 46.84Ω , and 48.5Ω at $d = 0.5\text{cm}$, 1cm , and 1.5cm , respectively, being very close to the corresponding simulated resistances of 44.54Ω , 46.13Ω , and 52.51Ω . It can be seen from Table 3.3 (a) that the use of matching capacitors has also effectively minimized the input reactances of the parallel plates to nearly zero. Measurements show that the addition of the matching capacitors has reduced the input reactances from 3.22Ω , 12.8Ω , and 2.73Ω to 1.23Ω , 0.3Ω , and -0.42Ω , measured at $d = 0.5\text{cm}$, 1cm , and 1.5cm respectively. They agree well with the simulated data where the input reactances have been decreased from 4.46Ω , 14.1Ω , and 4.08Ω to -1.54Ω , 0.75Ω , and -1.57Ω , measured at the same distances. The pairs of matching capacitors are found to have the similar effect on the output resistance and reactance of the parallel plates, as can be observed in Table 3.3 (b). Including a pair of matching capacitors at the input and output ports causes the output resistance to increase. It minimizes the output reactance of the parallel plates at the same time, easing connection with other $50\text{-}\Omega$ electronic systems. Slight deviation between the measured and simulated data is potentially caused by component tolerance of the capacitors, which is about 5%.

Table 3.3: Measured and simulated impedances of the equal plates configuration ($L_1 = L_2 = 15\text{cm}$) at different d : (a) Input impedance. (b) Output impedance.

d (cm)	Input resistance, R_{in} (Ω)				Input reactance, X_{in} (Ω)			
	Without matching capacitors		With matching capacitors		Without matching capacitors		With matching capacitors	
	Sim.	Exp.	Sim.	Exp.	Sim.	Exp.	Sim.	Exp.
0.5	4.84	5.39	44.54	47.28	4.46	3.22	-1.54	1.23
1	3.51	3.88	46.13	46.84	14.10	12.80	0.75	0.30
1.5	3.40	3.65	52.51	48.50	4.08	2.73	-1.57	-0.42

(a)

d (cm)	Output resistance, R_{out} (Ω)				Output reactance, X_{out} (Ω)			
	Without matching capacitors		With matching capacitors		Without matching capacitors		With matching capacitors	
	Sim.	Exp.	Sim.	Exp.	Sim.	Exp.	Sim.	Exp.
0.5	4.83	5.25	53.84	45.72	8.83	6.06	-0.56	1.77
1	3.09	3.49	48.64	43.35	12.00	10.44	3.76	3.08
1.5	2.90	3.06	40.72	33.99	9.12	6.11	1.43	1.49

(b)

Now for the $L_1 = L_2$ case ($d = 0.5\text{cm}$ and $D = 0.5\text{cm}$), parametric analysis is performed on both C_1 and C_2 . By keeping $C_2 = 47\text{pF}$, the capacitance C_1 is analyzed first. In this case, the corresponding input and output impedances are recorded for every combination of C_1 and C_2 at its respective operating frequency (at maximum $|S_{21}|$). The simulated result is shown in Fig. 3.7 (a). From Fig. 3.7 (a), it can be seen that the input resistance decreases from 81.9Ω to 20.23Ω while the output resistance

increases from 29.86Ω to 114.09Ω , as C_1 is raised from 20pF to 65pF . It is interesting to observe from the figure that the curves for the two resistances crossed at around $C_1 = 35\text{pF}$, the capacitance at which R_{in} and R_{out} becoming close to 50Ω . However, capacitor of value 35pF is not practically available and thus, another capacitance which is closest to 35pF with lowest tolerance (39pF) is chosen instead in experiment. With reference to Fig. 3.7 (a), the reactance is well below 3Ω for all capacitance values. Also, the maximum $|S_{21}|$ reads -0.1283dB at $C_1 = 35\text{pF}$ at the input impedance $R_{in} = 50.83 - j0.97\Omega$ and output impedance $R_{out} = 47.33 - j0.52\Omega$, both of which are quite close to 50Ω , as shown in Fig. 3.7 (b). This is because simultaneous bilateral matching has been achieved at both the input and output ports. The operating frequency decreases from 215.6MHz to 186.8MHz as C_1 is increased from 20pF to 65pF .

With $C_1 = 39\text{pF}$ unchanged, next, the effect of C_2 on the corresponding impedances, maximum $|S_{21}|$, and operating frequencies is again studied for the same case in Fig. 3.8. With reference to Fig. 3.8 (a), C_2 does affect the input and output resistances. The input resistance increases from 39.11Ω to 60.43Ω and the output resistance decreases from 61.07Ω to 38.01Ω when C_2 is increased from 30pF to 70pF . For both, their rate of change is much lesser than the previous case. As C_2 is varied from 30pF to 70pF , the reactance falls within the range of -2Ω to 1Ω . Referring to Fig. 3.8 (b), the maximum $|S_{21}|$ falls on $C_2 = 55\text{pF}$. At this capacitance, the input and output impedances are $49.58 - j0.79\Omega$ and $48.25 - j0.36\Omega$ respectively, quite close to the system characteristic impedance of 50Ω for many wireless electronics. With reference to the same figure, the operating frequency decreases from 210.8MHz to 185MHz as C_2 is increased from 30pF to 70pF . Adding two matching capacitors C_1

and C_2 to the input and output ports of the parallel plates can, obviously, change the input and output impedances, lifting them up close the system impedance ($\sim 50\Omega$), with negligible reactance. It has been shown that both the ports can be simultaneously transformed to 50Ω .

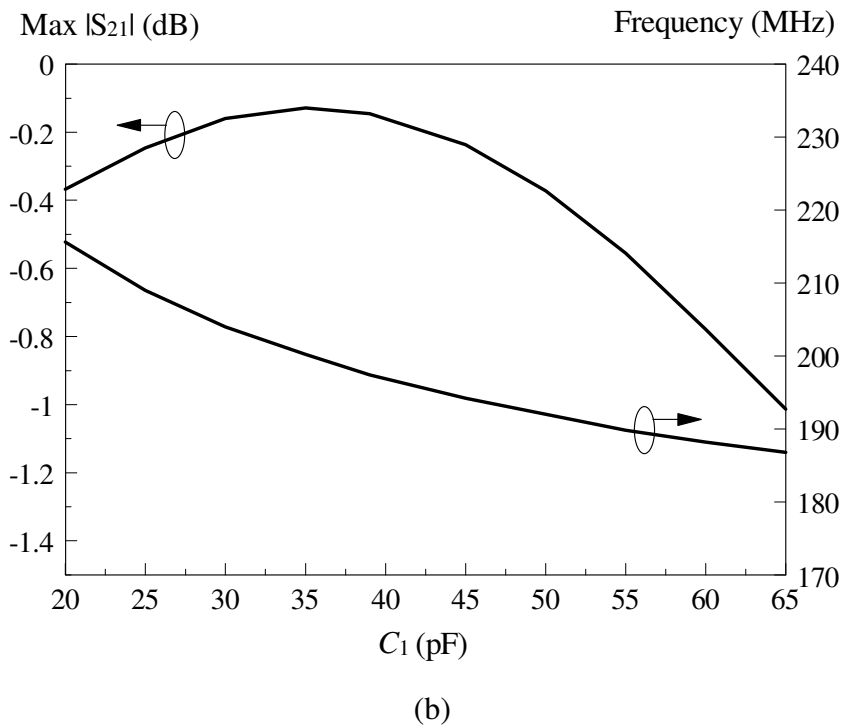
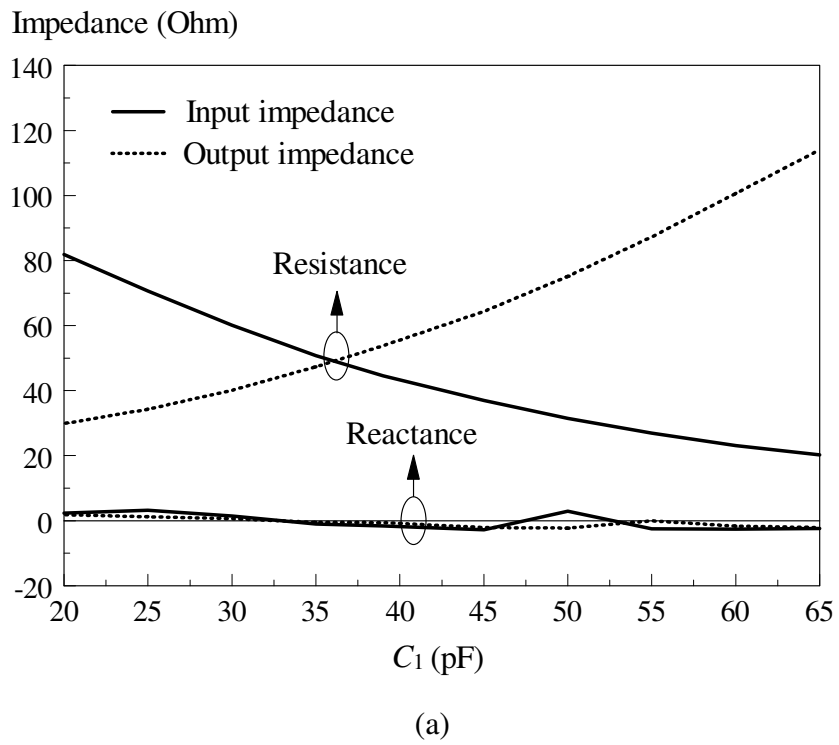
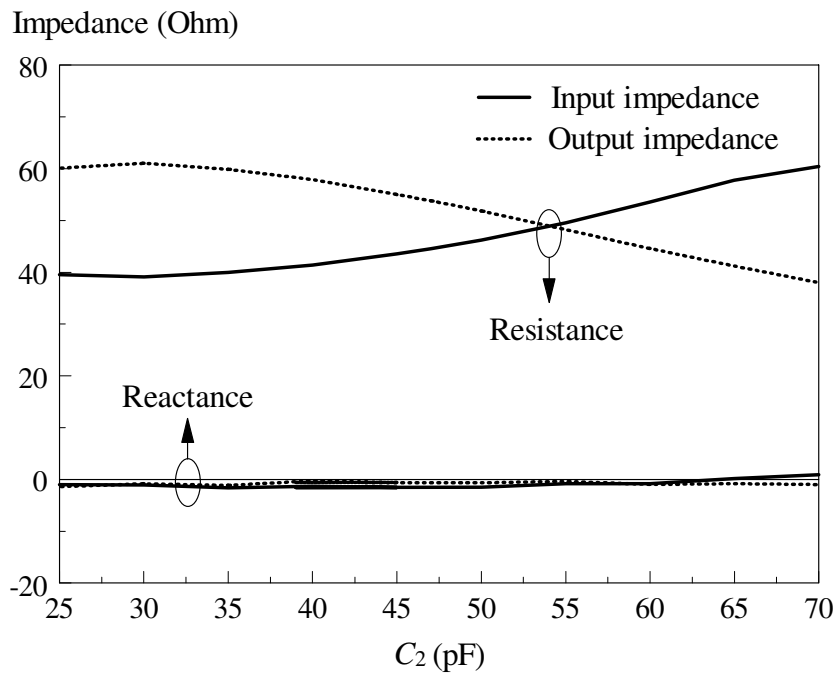
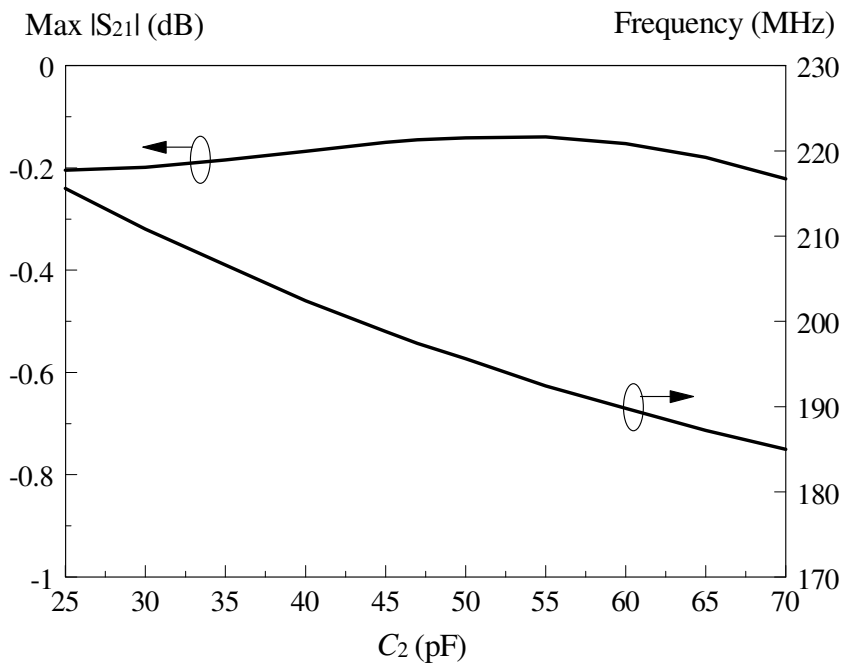


Figure 3.7: Effect of C_1 on the equal plates configuration ($L_1 = L_2 = 15\text{cm}$): (a) Input and output impedances. (b) Maximum $|S_{21}|$ and operating frequencies.



(a)



(b)

Figure 3.8: Effect of C_2 on the equal plates configuration ($L_1 = L_2 = 15\text{cm}$): (a) Input and output impedances. (b) Maximum $|S_{21}|$ and operating frequencies.

The size of the internal plates is now reduced to $L_2 = 7.5\text{cm}$, with other parameters as $L_1 = 15\text{cm}$, $d = 1\text{cm}$, and $D = 0.5\text{cm}$. Capacitors $C_1 = 56\text{pF}$ and $C_2 = 3\text{pF}$ are used to achieve impedance matching at both the input and output ports. Fig. 3.9 shows the simulated and measured S parameters, with the corresponding input impedances depicted for port 1. With reference to the figure, the measured and simulated operating frequencies at maximum $|S_{21}|$ are found to be 220.25MHz and 215.8MHz respectively, with a slight error of 2.06%. In this case, the corresponding $|S_{21}|$ is measured to be -1.534dB, slightly lower than the simulated one of -0.8845dB. The discrepancies between the measured and simulated operating frequencies and maximum $|S_{21}|$ are potentially caused by the tolerance of the matching capacitors C_1 and C_2 . The tolerance of $C_1 = 56\text{pF}$ is $\pm 10\%$ and $\pm 0.25\text{pF}$ for $C_2 = 3\text{pF}$. These tolerances in the matching capacitors will cause a shift of operating frequency and input and output impedance mismatches of the CWPT model. Consequently, the coupling efficiency, $|S_{21}|$ will degrade. From this information, the simulated PTE is calculated to be 81.57%. Spectrum measurement gives a PTE of 81.66%. It is worth to mention that the measured PTE for this configuration is only 9.33% lower than that of the equal plates.

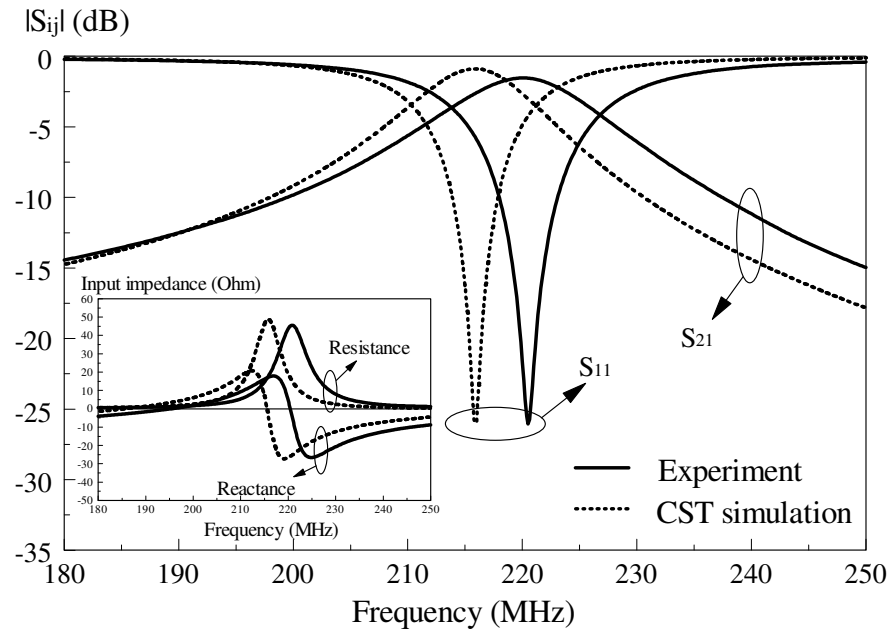


Figure 3.9: Measured and simulated S parameters for the parallel plates with $L_1 = 15\text{cm}$, $L_2 = 7.5\text{cm}$, $d = 1\text{cm}$, and $D = 0.5\text{cm}$. The corresponding measured and simulated input impedances are shown in the inset.

Fig. 3.10 is a photo showing the experimental setup for the equal plates system, where $L_1 = L_2 = 15\text{cm}$, $d = 0.5\text{cm}$, $D = 0.5\text{cm}$, and $C_1 = 39\text{pF}$, $C_2 = 47\text{pF}$. The output load at the internal plates is now replaced by an LED (with negligible resistance). A $51\text{-}\Omega$ lumped resistor is soldered in parallel with the LED to provide voltage drop. The ac power is supplied by a signal generator to the outer plates. As can be seen from the figure, the wireless power transfer from the plates has successfully provided enough power to the LED for lighting it up.

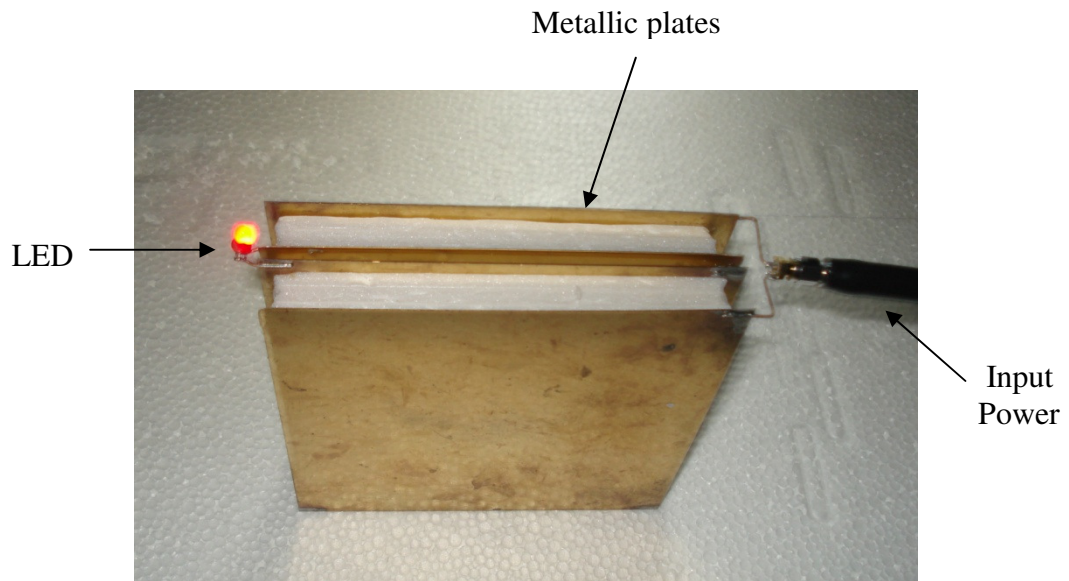


Figure 3.10: Photograph showing the equal plates system ($L_1 = L_2 = 15\text{cm}$, $d = 0.5\text{cm}$, $D = 0.5\text{cm}$, and $C_1 = 39\text{pF}$, $C_2 = 47\text{pF}$) for lighting up LED.

3.4 Conclusion

Parallel plates system has been proposed for transferring wireless power to the electronic components and integrated circuits (IC) on the computer peripherals. Two configurations have been demonstrated achieving a power transfer efficiency of greater than 80%. Also, simultaneous impedance matching has been achieved at both the input and output ports. This method has great potential to be deployed to supply power to the peripherals of the computer motherboard in the future.

CHAPTER 4

CAPACITIVE WIRELESS POWER TRANSFER FOR ON-CHIP APPLICATIONS

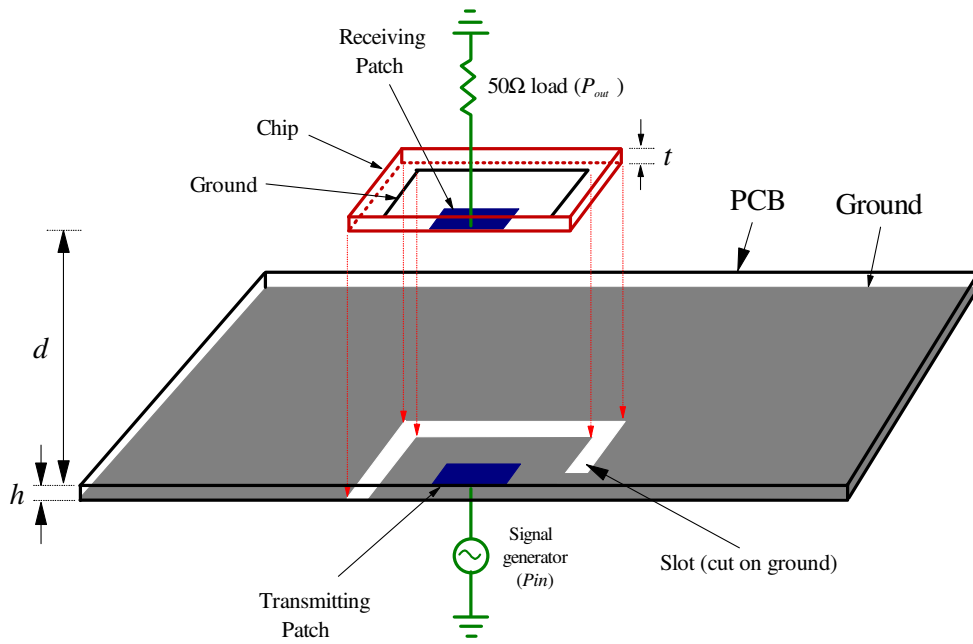
4.1 Introduction

The past decade has witnessed the rapid improvement in the processing speed of integrated circuits (IC). The component size has continuously scaled down along with the surge of operating frequency. Beyond a certain frequency especially in millimeter-wave ranges, signal transmission and power transfer through metallic interconnects can become very inefficient due to high conductive and dielectric losses. Over the past decades, tremendous effort has been made to improve the interconnect performance by reducing the material resistivity and dielectric loss of the transmission line. This is, however, not fast enough to catch up with the rapid increase of circuit size, which may require the usage of thousands or millions of interconnects. Instead of using metal to make interconnects, for the first time in this dissertation, the capacitive wireless power transfer (CWPT) is deployed for transmitting electric power to a metallic patch on a chip. For demonstration, the patch is made on a single piece of substrate, which is cut into the shape of a chip package.

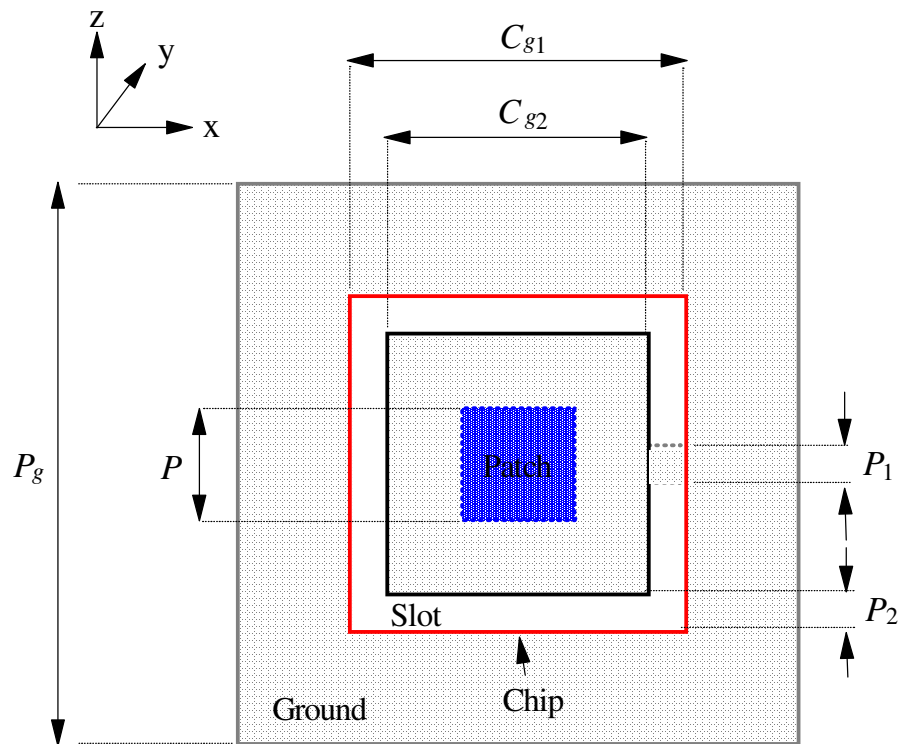
4.2 Capacitive Wireless Power Transfer Configuration

The capacitive wireless power transfer (CWPT) model proposed in this chapter is an extended application of CWPT model demonstrated in *Chapter 2*. The method is now adopted for on-chip application. Fig. 4.1(a) and (b) show the profile view of the model cutting through its chip centre and the corresponding top view. It has a dimension of $h = 1.6\text{mm}$, $d = 0.5\text{mm}$, $t = 1.27\text{mm}$, $C_{g1} = 60\text{mm}$, $C_{g2} = 51\text{mm}$, $P_g = 160\text{mm}$, $P = 27.6\text{mm}$, $P_1 = 4\text{mm}$ and $P_2 = 4.5\text{mm}$.

It is observed that this structure is close to that in Chapter 2, except that now the metallic patches are made on dielectric substrates. With reference to Fig. 4.1(a), the bottom substrate (with dielectric constant of $\epsilon_r = 4.4$) is a PCB which has a ground plane on its bottom layer. The transmitting patch, soldered to the inner conductor of a coaxial connector, is made on the top surface of the PCB. The external conductor of the connector is connected to the ground plane. A microwave signal generator (R&S SMB 100A with $Z_o = 50\Omega$) is used to supply input power (P_{in}). With reference to the figure, the chip is cut out of a high-permittivity ($\epsilon_r = 10.2$) substrate with the receiving patch etched on the bottom surface of it. The top surface of the chip has a ground plane functioning as a return path. As can be seen from the figure, the harvested power (P_{out}) is channelled to a 50Ω load going through a coaxial connector. In order to achieve maximum electric field coupling between the transmitting and receiving patches, they are made to have the same size.



(a)



(b)

Figure 4.1: The proposed CWPT scheme for on-chip applications: (a) Profile view. (b) Top view.

It is interesting to note that part of the ground plane around the PCB has been removed to form a C-shaped slot. The effect of this slot will be studied in detail in *Section 4.3*.

Besides the proposed configuration in Fig. 4.1, another on-chip CWPT scheme which has an embedded substrate ($\epsilon_r = 10.2$ and $t_1 = 0.635\text{mm}$) between the patches, is proposed. The configuration is shown in Fig. 4.2. All other design parameters of the configuration in Fig. 4.2 are identical to those in Fig. 4.1.

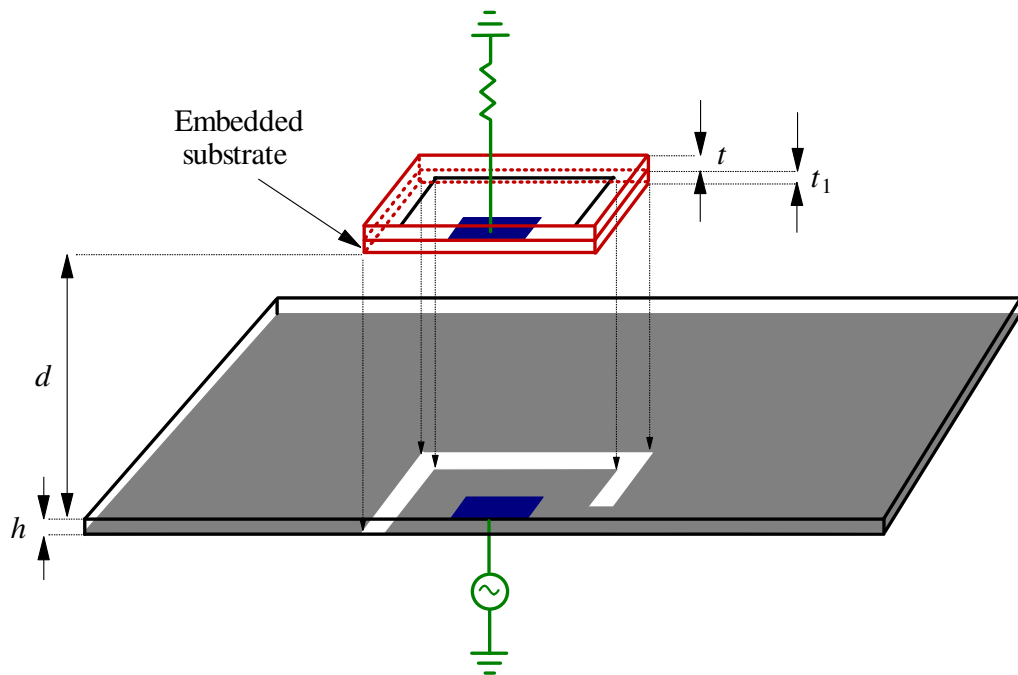


Figure 4.2: On-chip CWPT scheme with an embedded substrate between the patches.

4.3 Results and Discussion

The proposed CWPT simulation models were constructed on the CST Microwave Studio. In experiment, the S parameters were measured using a ZVB8 vector network analyzer. To measure the power transfer efficiency (PTE), a 50- Ω SMB100A signal generator coupled with a 50 Ω FSL spectrum analyzer are used.

4.3.1 Power Transfer Efficiency

The CWPT scheme shown in Fig. 4.1 will be described first. Fig. 4.3 shows the simulated and measured S parameters as a function of frequency. The corresponding input impedances are depicted in the inset. Reasonable agreement is observed between the measured operating frequency (maximum $|S_{21}|$) of 2.82GHz and the simulated one of 2.866GHz, with an error of 1.61%. At their respective operating frequencies, the measured maximum $|S_{21}|$ is -2.373dB, which is slightly higher than that for simulation -2.405dB. The measured and simulated input impedances are $44.16 + j44.23\Omega$ and $45.81 + j32.68\Omega$, respectively, at the operating frequencies. For both, the reactances are high as no impedance matching has been made at the input and output ports. The simulated maximum $|S_{21}|$ of -2.405 dB implies a calculated PTE of 57.48% ($\text{PTE} = |S_{21}|^2 \times 100\%$) at the operating frequency. Measurement shows that the PTE at 2.82GHz is 55.45%, which is only 2.03% lower than simulation. Low PTE is seen and it is probably caused by the large input reactance which can lead to impedance mismatch between the source and the patches.

In experiment, the small gap between the power receiving and transmitting patches ($d = 0.5$ mm) is maintained by inserting several small pieces of substrate of thickness 0.5 mm and relative dielectric constant of 2.2 in between the chip and PCB. The discrepancies between the measured and simulated $|S_{11}|$ and operating frequencies are potentially caused by these embedded substrates. Such discrepancies are directly related to the difference between measured and simulated input reactances.

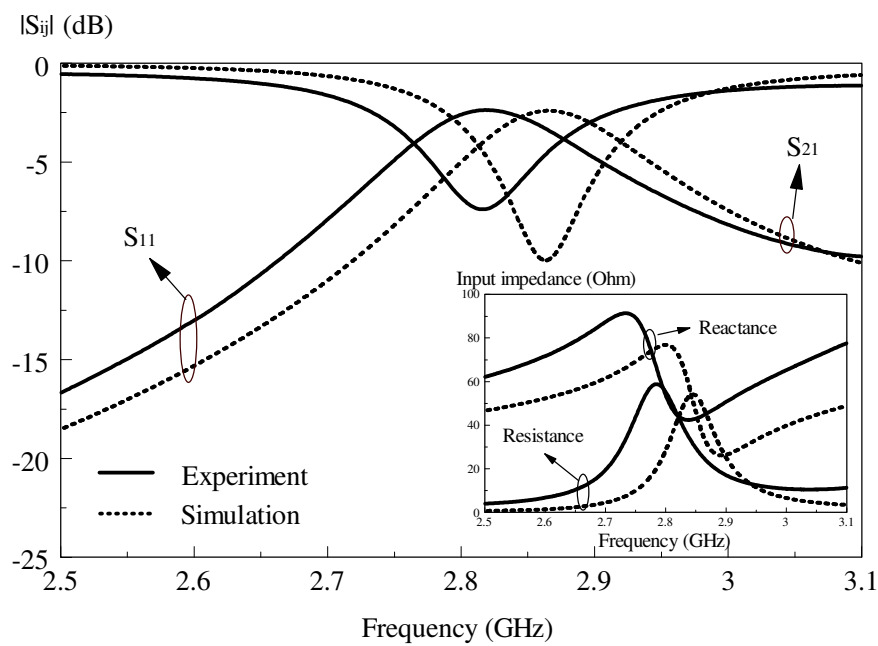


Figure 4.3: Simulated and measured S parameters of the CWPT model in Fig. 4.1. The inset shows the corresponding simulated and measured input impedances.

Fig. 4.4 shows the S parameters of CWPT configuration shown in Fig. 4.2, along with their corresponding input impedance depicted in the inset. The measured and simulated operating frequencies are 2.745GHz and 2.729GHz, respectively, with an error of 0.59%. The measured maximum $|S_{21}|$ is -2.615dB, which is slightly higher

than the simulated one of -3.059dB at their respective operating frequencies. From -3.059dB , the simulated PTE is calculated to be 49.44% . Measurement shows that the actual PTE is 50.12% , which is 0.68% higher than simulation.

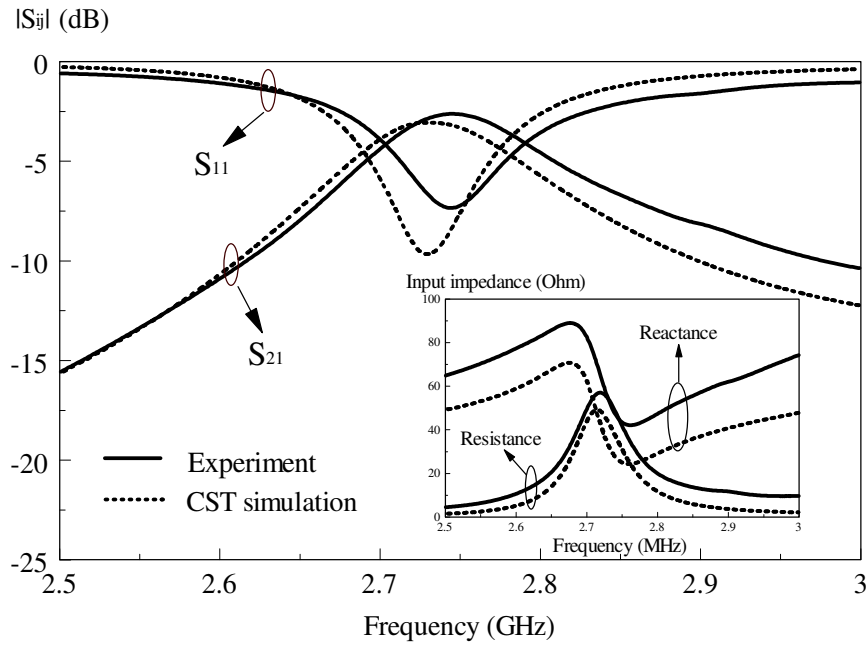


Figure 4.4: Simulated and measured S parameters of the CWPT model with an embedded layer between the two patches (Fig. 4.2). The inset shows the corresponding simulated and measured input impedances.

Comparing to the configuration without embedded substrate (Fig. 4.1), the PTE of the CWPT configuration depicted in Fig. 4.2 has a lower measured PTE of 5.33% . The drop can be due to the increase in distance between the transmitting and receiving plates (from $d = 0.5\text{mm}$ to $d + t_l = 1.135\text{mm}$).

4.3.2 Dielectric Breakdown Voltage

In practical applications, it is essential to know the allowable maximum voltage that can be applied to an electronic or electrical system to prevent any damages due to voltage breakdown. Both of the proposed CPWT configurations in this chapter are actually parallel-plate capacitor in nature. Such capacitor has an inherent breakdown voltage V_{bd} , at which the dielectric in between the parallel plates becomes conductive, causing a short circuit between the plates. It is the maximum allowable voltage across the parallel plates before damaging the capacitor. The V_{bd} of a parallel-plate capacitor is decided by the dielectric material and separation distance between the plates d , where $V_{bd} = E_{ds}d$. The parameter E_{ds} is defined as the dielectric strength - the magnitude of electric field at which dielectric breakdown occurs.

For the CWPT model shown in Fig. 4.1, the dielectric in between the plates is air. In general, the E_{ds} for an air dielectric capacitor is in the order of 2 to 5kV/mm under normal conditions of pressure and temperature (Dyer 2001). This value mainly depends on d . Usually, E_{ds} is greater for smaller d . Other factors such as air pressure, humidity, temperature, frequency, duration of the applied voltage, as well as the shape and material of the plates also slightly affect E_{ds} . The E_{ds} value will get closer to 5kV/mm when d is made small enough (less than 1mm). Therefore, assuming that $E_{ds} = 5\text{kV/mm}$ and ignoring other factors, the V_{bd} for the CWPT configuration depicted in Fig. 4.1 (with $d = 0.5\text{mm}$) can be calculated as:

$$\begin{aligned} V_{bd} &= E_{ds}d \\ &= (5\text{kV/mm})(0.5\text{mm}) \end{aligned}$$

$$= 2.5\text{kV}$$

It should be reminded that there are two more parallel-plate capacitor-like structures in CWPT model shown in Fig. 4.1. The first one is formed by the transmitting patch and the PCB ground while the second is formed by the receiving patch and the chip ground. As the transmitting patch is made on the FR4 substrate, by knowing the dielectric strength $E_{FR4} = 20\text{kV/mm}$ (Vidhale and Khanapurkar 2012) and the thickness of the PCB to be $h = 1.6\text{mm}$, the V_{bd} can be calculated as:

$$\begin{aligned} V_{bd} &= E_{FR4} h \\ &= (20\text{kV/mm})(1.6\text{mm}) \\ &= 32\text{kV} \end{aligned}$$

The material used for the chip is Rogers 6010 substrate which has a dielectric strength of $E_{6010} = 16\text{kV/mm}$ (Chang 2000). The distance between the receiving patch and chip ground is 1.27mm. Therefore, the breakdown voltage V_{bd} can be calculated as:

$$\begin{aligned} V_{bd} &= E_{6010} t \\ &= (16\text{kV/mm})(1.27\text{mm}) \\ &= 20.32\text{kV} \end{aligned}$$

4.3.3 Studies on Impedance and Power Transmission

Several groups of simulations will be performed to study the characteristics of the CWPT configuration shown in Fig. 4.1, focusing on the operating frequency and their corresponding power transfer efficiency. Although the predominant system impedance of most of the contemporary electronic and wireless systems is 50Ω , some are still using other values such as 75Ω . Therefore, the responses of maximum $|S_{21}|$ and operating frequency to different values of load impedance Z_L are investigated. The result is shown in Fig. 4.5. As the CWPT configuration has been optimized for $Z_L = 50\Omega$, it is expected to have highest $|S_{21}|$ in the vicinity of $Z_L = 50\Omega$. With reference to Fig. 4.5, it is noted that $|S_{21}|$ peaks at $Z_L = 40\Omega$ with $|S_{21}| = -2.38\text{dB}$, which is slightly higher than $|S_{21}| = -2.405\text{dB}$ when $Z_L = 50\Omega$. The maximum $|S_{21}|$ value decreases slowly to -3.099dB as Z_L is increased from $Z_L = 50\Omega$ to 150Ω . This is very positive as it shows that the proposed CWPT can be used for a wide range of Z_L value. When Z_L is in $50\Omega - 150\Omega$, the operating frequency falls in the range of $2.85\text{GHz} - 2.95\text{GHz}$.

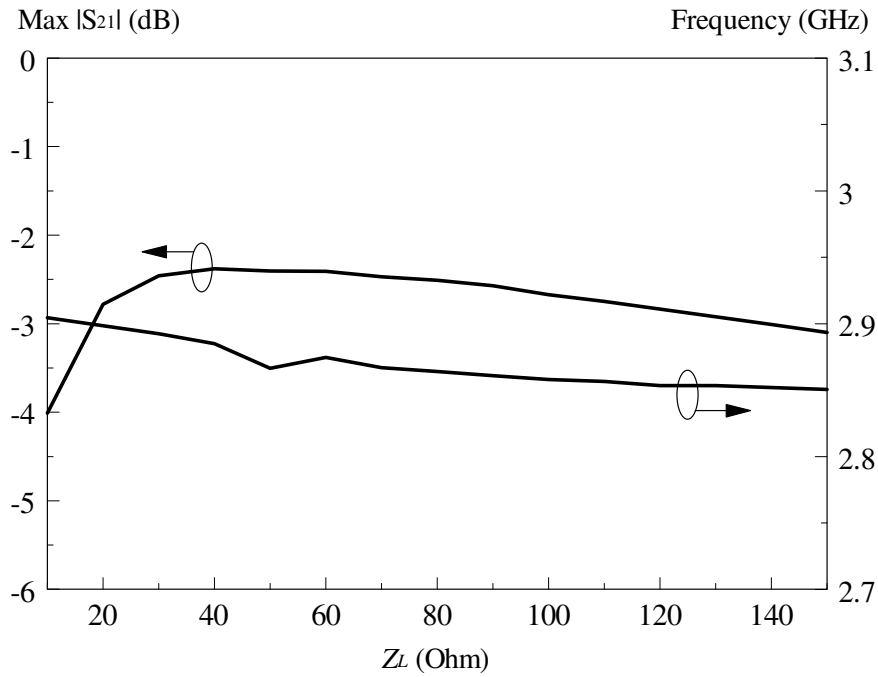


Figure 4.5: Effect of the load impedance Z_L on the maximum $|S_{21}|$ and operating frequency of the CWPT in Fig. 4.1.

Next, the distance between the plates d is varied and the corresponding operating frequency and maximum $|S_{21}|$ are plotted as a function of d , as shown in Fig. 4.6. With reference to the figure, it is observed that the maximum value of $|S_{21}|$ drops from -2.028dB to -4.499dB while the operating frequency increases from 2.711GHz to 3.124GHz as d is increased from 0.3mm to 1.2mm . The amplitude drop is expected as electric field attenuates faster with farther distance.

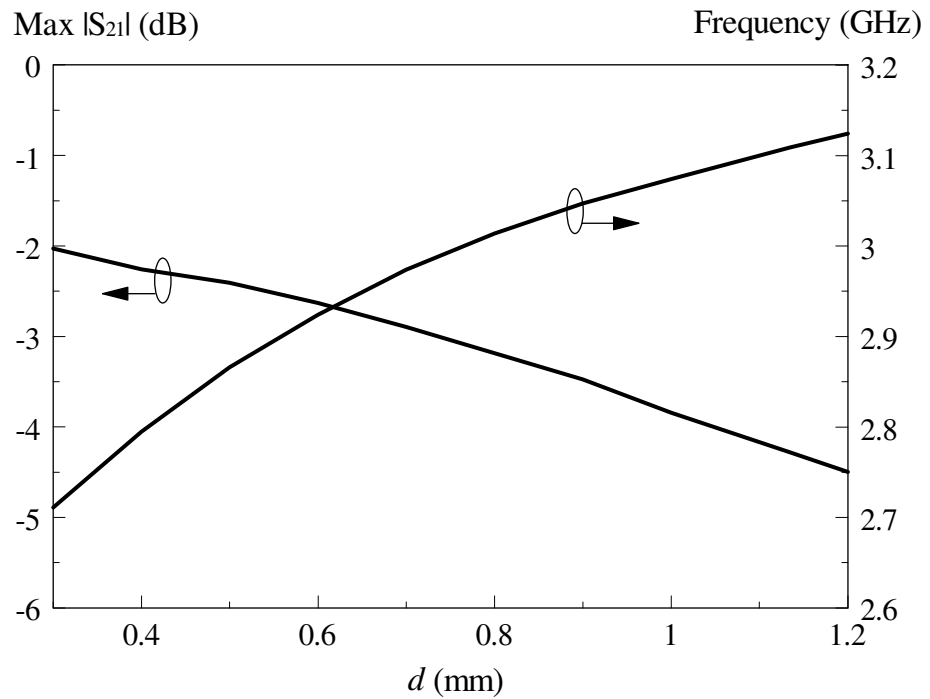


Figure 4.6: Effect of the distance between patches d on the maximum $|S_{21}|$ and operating frequency.

Here, the effect of the patch size is studied in Fig. 4.7. It can be seen that $|S_{21}|$ has a maximum value at $P = 30\text{mm}$. The transmitting and receiving plates are designed to have the same size to achieve optimum electric field coupling efficiency between them. It is observed that the operating frequency decreases from 2.962GHz to 2.443GHz gradually as P is increased from 22mm to 36mm . This is because larger plates result in a lower resonant frequency, as expected.

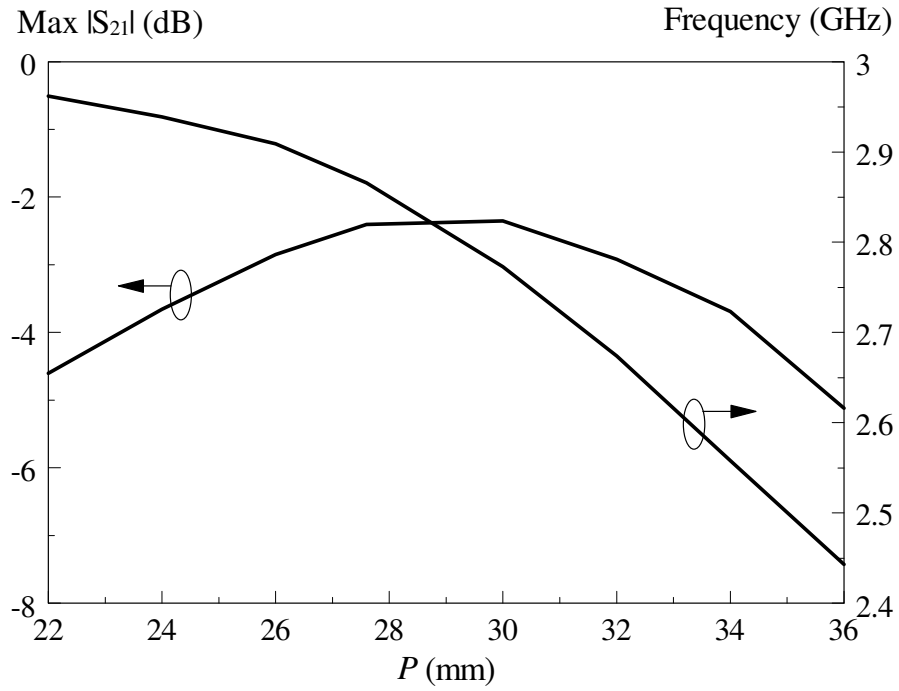
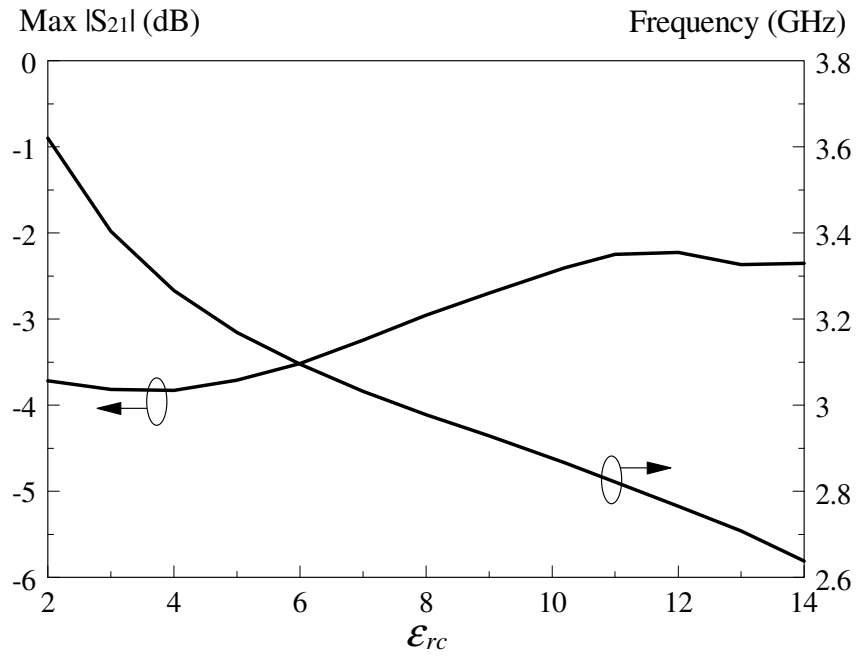
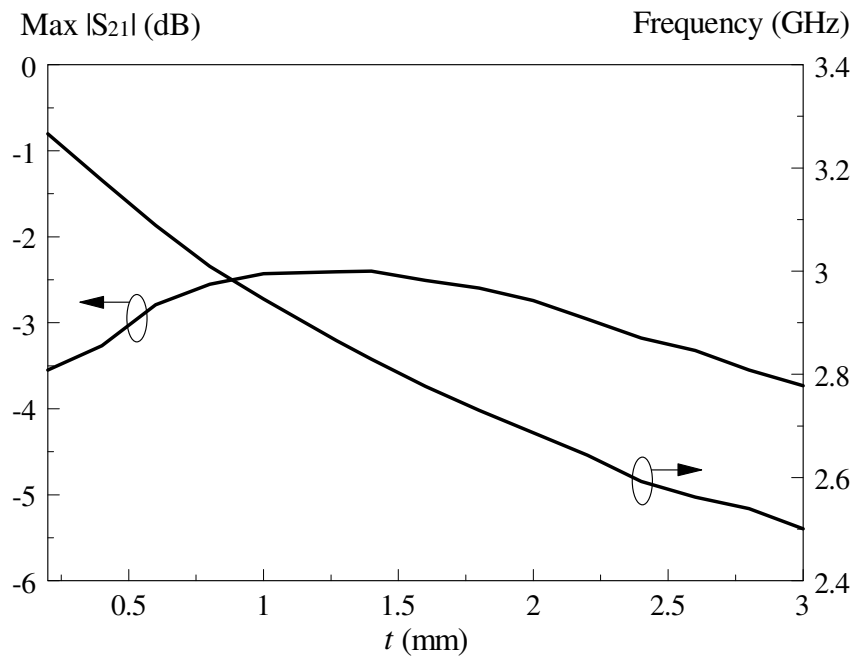


Figure 4.7: Effect of plate size on the maximum $|S_{21}|$ and operating frequency.

The effects of the chip permittivity (ϵ_{rc}) and thickness (t) are now studied in Fig. 4.8(a) and (b), respectively. With reference to Fig. 4.8(a), the operating frequency decreases from 3.62GHz to 2.638GHz as ϵ_{rc} is increased from 2 to 14. The transmission coefficient $|S_{21}|$ peaks at -2.227dB at the chip permittivity of $\epsilon_{rc} = 12$. It is found from Fig. 4.8 (b) that the operating frequency decreases with increasing t . Also observed is that $|S_{21}|$ reaches its maximum magnitude of -2.399dB at $t = 1.4$ mm.



(a)



(b)

Figure 4.8: Effect of chip material on the maximum $|S_{21}|$ and operating frequency:

(a) Relative dielectric constant ϵ_{rc} . (b) Thickness t .

Fig. 4.9 shows the effect of the chip ground size C_{g2} on the maximum $|S_{21}|$ and operating frequency. The operating frequency is found to be decreasing with increasing C_{g2} . The transmission coefficient $|S_{21}|$ changes with C_{g2} . It peaks at $C_{g2} = 50\text{mm}$ with a value of -2.337dB . This parameter can be used to optimize the $|S_{21}|$ and resonance of the CWPT. Simulation shows that $|S_{21}|$ and operating frequency are not affected by the chip size.

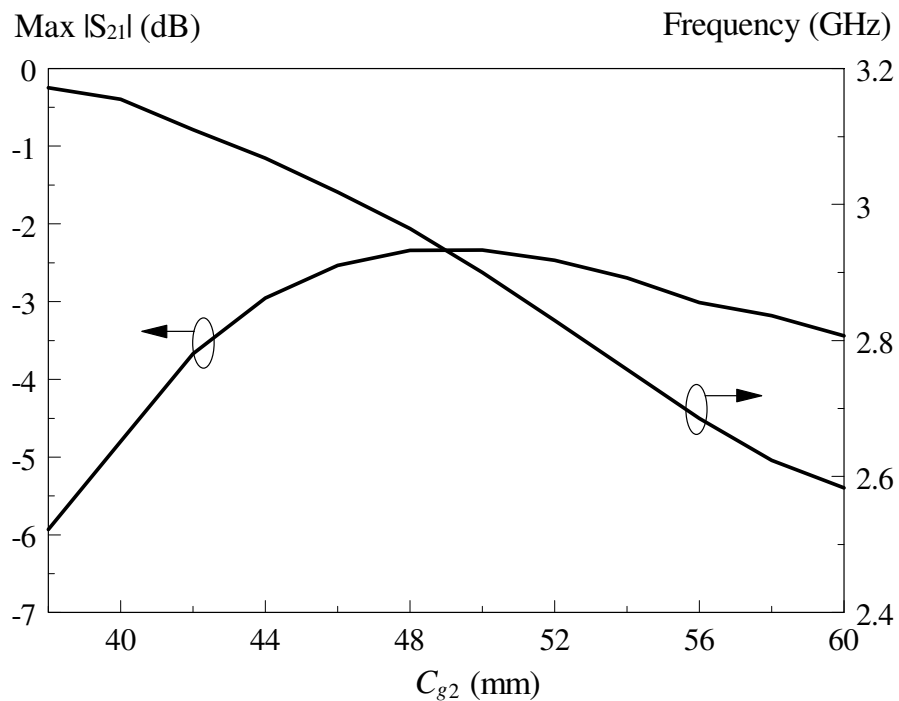
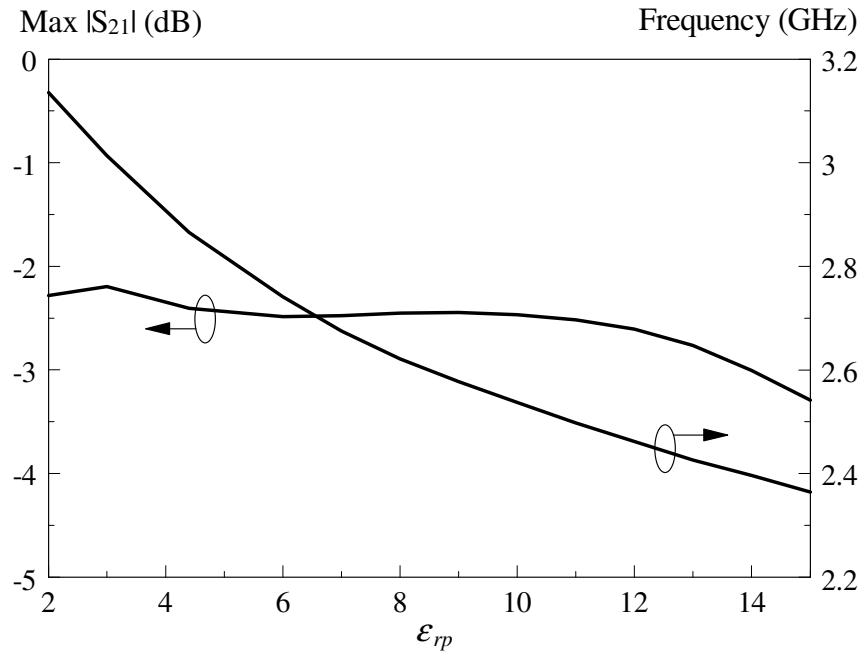


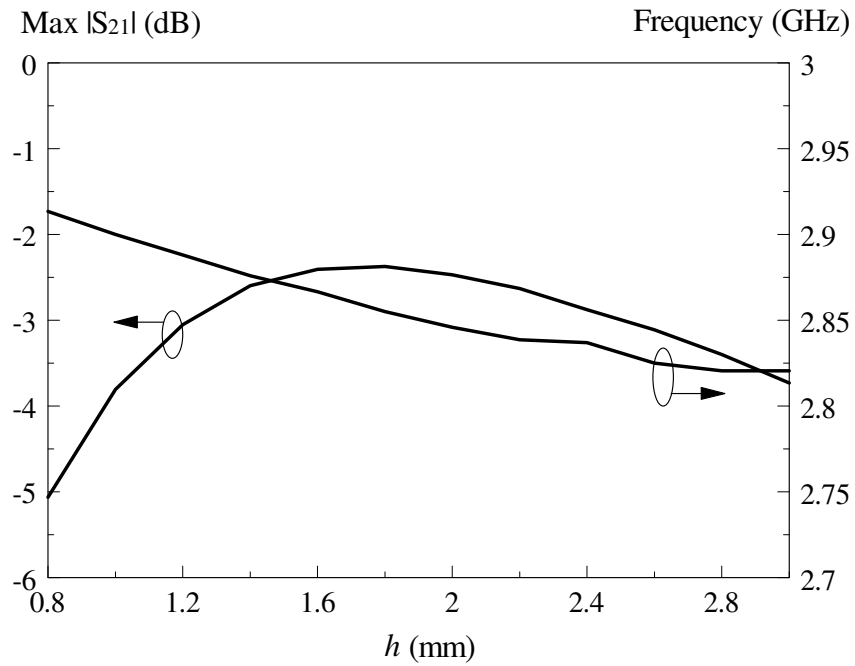
Figure 4.9: Effect of the ground size C_{g2} on the maximum $|S_{21}|$ and operating frequency.

The effect of the properties of the PCB material on the performance of the CWPT configuration will now be studied as well. Fig. 4.10 (a) and (b) show the changes of $|S_{21}|$ and operating frequency when the relative dielectric constant ϵ_{rp} and thickness h of the PCB are varied. With reference to Fig. 4.10 (a), the maximum $|S_{21}|$

is found to be varying inconsistently with the ϵ_{rp} of the PCB and reaching its maximum of -2.194dB at $\epsilon_{rp} = 3$. The operating frequency decreases with increasing ϵ_{rp} . In Fig. 4.10 (b), it can be seen that the thickness $h = 1.8\text{mm}$ produces the highest $|S_{21}|$ of -2.372dB. The operating frequency decreases as h is increased. Simulation shows that the PCB size including its ground plane has negligible effect on $|S_{21}|$ and operating frequency as long as it is larger than the chip. This implies that the chip can be placed at any location on the PCB.



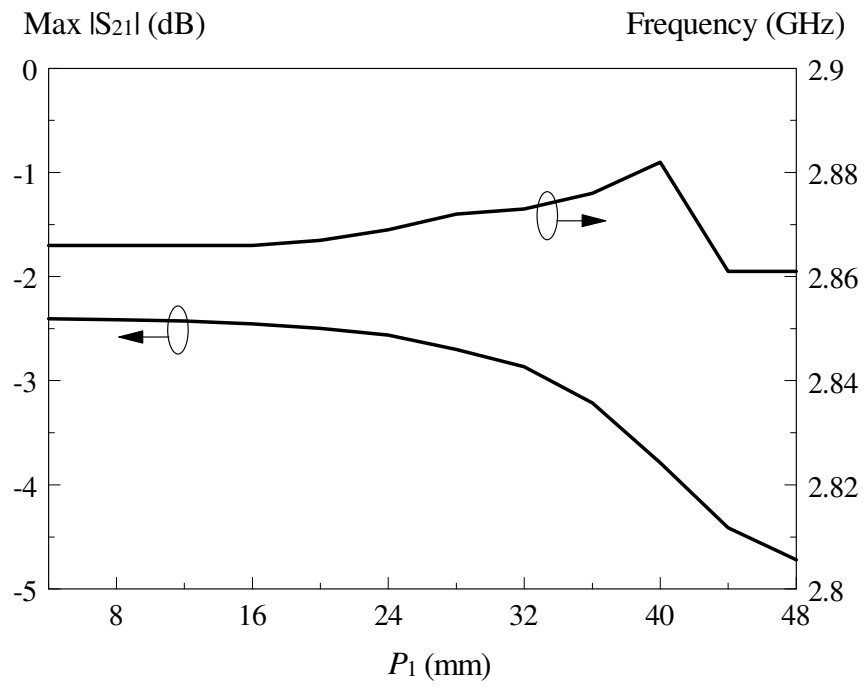
(a)



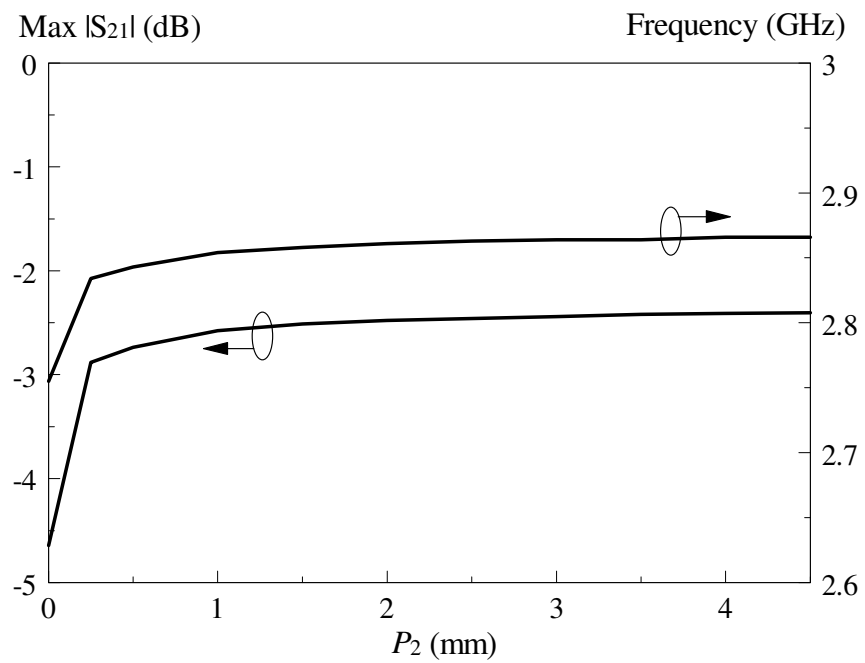
(b)

Figure 4.10: Effect of the PCB material on the maximum $|S_{21}|$ and operating frequency: (a) Relative dielectric constant ϵ_{rp} . (b) Thickness h .

Finally, the effect of the C-shaped slot is studied. With reference to Fig. 4.2(b), the line width P_1 is varied along the center line of the chip, and the corresponding maximum $|S_{21}|$ and operating frequency are recorded in Fig. 4.11(a). Referring to the figure, $|S_{21}|$ decreases from -2.405dB to -4.719dB as P_1 is increased from 4mm to 48mm. A better power transfer can be obtained by narrowing the line width. The operating frequency changes inconsistently within the frequency range of 2.861GHz - 2.882GHz. The second parameter to be analyzed is P_2 , shown in Fig. 4.11 (b). The P_2 value is varied from 0 to 4.5mm. No gap exists for $P_2 = 0$, implying an all-filled-up ground plane. With reference to Fig. 4.11(b), $|S_{21}|$ decreases gradually as P_2 becomes smaller. At $P_2 = 0$ (no gap), $|S_{21}|$ drops significantly to -4.641dB. This shows that the existence of the C-shaped slot is crucial for optimizing the power transfer between the patches. The operating frequency is found to be increasing with increasing P_2 .



(a)



(b)

Figure 4.11: The effect of the dimension of the C-shaped slot on the maximum $|S_{21}|$ and operating frequency: (a) P_1 . (b) P_2 .

4.4 Conclusion

For the first time, the capacitive coupling mechanism has been explored for transferring wireless power to chips and ICs. In this chapter, two capacitive wireless transfer schemes have been proposed and studied. The design parameters have been analyzed. To understand the voltage management ability of the proposed CWPT configuration, the dielectric breakdown voltage is calculated. As metallic interconnects is lossy at very high frequency ranges, this idea provides a potential solution to it.

CHAPTER 5

SUMMARY AND FUTURE WORK

5.1 Summary

In this dissertation, three capacitive wireless power transfer (CWPT) schemes have been proposed. They are intended for mid-range WPT, computer peripherals and on-chip applications. The commercial software CST Microwave Studio was used to simulate all the proposed configurations. The simulation results were then verified by experiments. Good agreement was observed between the simulation and measurement results. The research highlights in this dissertation are re-summarized as follows:

- i) A novel CWPT scheme has been demonstrated by using a pair of parallel plates. It produces a better power transfer efficiency (PTE) than a pair of coils in the same frequency range. The association of a large ground plate with each of the plates can improve the PTE significantly. The plate size can be optimized for the best possible PTE performance. Near-distance simultaneous power transfer to multiple parallel plates can be easily realized with very low electromagnetic interference.
- ii) Next, a new way to transfer wireless power to the computer peripheral is proposed using electric field coupling. Capacitive patches are made on the chip package or PCB to harvest power from a pair of parallel plates. This is a good

solution to power up the electronics on a peripheral board in bulk. It has been demonstrated that the input and output ports of the parallel plates system can both achieve good impedance matching at the same time.

- iii) Finally, the CWPT method will be applied for on-chip applications. It is used to transfer power to chip placed on top of a PCB through wireless mechanism at microwave frequency. This idea can provide a potential solution for future on-chip power transfer as metallic interconnects can become very lossy at very high frequency.

5.2 Future Work

This dissertation has successfully proposed and studied three new methods for CWPT. The proposed ideas are potentially useful for transferring power to various portable and mobile electronic devices and communication systems. In future, semiconductor technologies should be considered to miniaturize the proposed CWPT models at high frequency.

As mentioned earlier, no impedance matching scheme was applied to the CWPT model introduced in *Chapter 2*. The impedance mismatch gets worse as the distance between the power transmitting and receiving plates, d increases, as shown in Fig. 2.5 (b). Therefore, drastic drop of PTE was observed as d increases. Such power loss is very undesirable in WPT as significant amount of input power is wasted. Thus, an efficient input and output impedance matching methodology must

be designed and deployed before this CWPT model can be applied practically for more efficient power transfer.

Over the past years, practical electronic circuit boards get more complex with significant increase of electronic components and ICs on a single package. Powering mechanism for such circuit boards becomes more complex and challenging. The CWPT model proposed in *Chapter 3* can be a potential solution for this problem. Using this scheme, powering up multiple electronic components on a circuit board is possible by embedding it in between a pair of sufficiently large metallic plates which act as source of power or power transmitting plates. By properly design the power receiving scheme for each of the component, power can be transferred efficiently from a single source of power (external plates) to the electronic components simultaneously.

As in the case of CWPT model proposed in *Chapter 2*, an efficient input and output impedance matching scheme is required to improve the PTE of on-chip CWPT model introduced in *Chapter 4*. By properly match the input and output impedances of the model to the source and load respectively, high PTE can be achieved even at very high frequency range at a near distance. In addition, power transfer from a single source or a power transmitting patch to multiple chips or receivers is possible by properly locate the receivers above the power transmitting patch with proper impedance matching.

References

Azad, U., Jing, H. C. and Wang, Y. E., 2012. Link budget and capacity performance of inductively coupled resonant loops. *IEEE Trans. Antennas Propag.*, 60 (5), pp. 2453-2461.

Bharj, S. S., Camisa, R., Grober, S., Wozniak, F. and Pendleton, E., 1992. High efficiency c-band 1000 element rectenna array for microwave powered applications. *IEEE MTT-S Int. Microwave Symp. Dig.*, pp. 301-303.

Brown, W. C., 1976. Optimization of the efficiency and other properties of the rectenna element. *IEEE MTT-S Int. Microwave Symp. Dig.*, 76 (1), pp. 142-144.

Brown, W. C., 1980. The history of the development of the rectenna. *Proc. SPS Microwave Syst. Workshop at JSC-NASA*, pp. 271-280.

Brown, W. C., 1984. The history of power transmission by radio waves. *IEEE Trans. Microwave Theory Tech.*, MTT-32 (9), pp. 1230-1242.

Brown, W. C. and Eves, E. E., 1992. Beamed microwave power transmission and its application to space. *IEEE Trans. Microwave Theory Tech.*, 40 (6), pp. 1239-1250.

Cannon, B. L., Hoburg, J. F., Stancil, D. D. and Goldstein, S. C., 2009. Magnetic resonant coupling as a potential means for wireless power transfer to multiple small receivers. *IEEE Trans. Power Electron.*, 24 (7), pp. 1819-1825.

Casanova, J. J., Low, Z. N. and Lin, J. S., 2009. A loosely coupled planar wireless power system for multiple receivers. *IEEE Trans. Ind. Electron.*, 56 (8), pp. 3060-3068.

Chang, K., 2000. *RF and microwave wireless systems*. New York: Wiley.

- Chen, Y. S., Chen, S. Y. and Li, H. J., 2010. Analysis of antenna coupling in near-field communication systems. *IEEE Trans. Antennas Propag.*, 58 (10), pp. 3327-3335.
- Cheon, S. H., Kim, Y. H., Kang, S. Y., Lee, M. L., Lee, J. M. and T. Y. Zyung, 2011. Circuit-model-based analysis of a wireless energy-transfer system via coupled magnetic resonances. *IEEE Trans. Ind. Electron.*, 58 (7), pp. 2906-2914.
- Chow, E. Y., Yang, C. L., Ouyang, Y. H., Chlebowski, A. L., Irazoqui, P. P. and Chappell, W. J., 2011. Wireless powering and the study of RF propagation through ocular tissue for development of implantable sensors. *IEEE Trans. Antennas Propag.*, 59 (6), pp. 2379-2387.
- Culurciello, E. and Andreou, A. G., 2006. Capacitive inter-chip data and power transfer for 3-D VLSI. *IEEE Trans. Circuits Syst. - II*, 53 (12), pp. 1348-1352.
- Dickinson, R. M., 1976. Performance of a high-power, 2.388-GHz receiving array in wireless power transmission over 1.54km. *IEEE MTT-S Int. Microwave Symp. Dig.*, pp. 139-141.
- Dyer, S. A., 2001. *Survey of instrumentation and measurement*. New York: Wiley-Interscience.
- Esser, A., 1995. Contactless charging and communication for electric vehicles. *IEEE Ind. Applications Mag.*, 1 (6), pp. 4-11.
- Ettorre, M. and Grbic, A., 2012. A transponder-based, nonradiative wireless power transfer. *IEEE Antennas Wireless Propag. Lett.*, 11, pp. 1150-1153.
- Fnato, H., Chiku, Y. and Harakawa, K., 2010. Wireless power distribution with capacitive coupling excited by switched mode active negative capacitor. *Int. Conf. on Electrical Machines and Syst.*, pp. 117-122.

Fu, W. Z., Zhang, B. and Qiu, D. Y., 2009. Study on frequency-tracking wireless power transfer system by resonant coupling. *IEEE 6th Int. Power Electron. and Motion Control Conf.*, pp. 2658-2663.

Hagerty, J. A., Helmbrecht, F. B., McCalpin, W. H., Zane, R. and Popovic, Z. B., 2004. Recycling ambient microwave energy with broadband rectenna arrays. *IEEE Trans. Microwave Theory Tech.*, 52 (3), pp. 1014-1024.

Hamam, R. E., Karalis, A., Joannopoulos, J. D. and Soljacic, M., 2009. Efficient weakly-radiative wireless energy transfer: An EIT-like approach. *Ann. Phys.*, 324, pp. 1783-1795.

Hatano, K., Shinohara, N., Mitani, T., Nishikawa, K., Seki, T. and Hiraga, K., 2011. Development of class-F load rectennas. *Proc. IMWS-IWPT 2011*, pp. 251-254.

Homma, Y., Sasaki, T., Namura, K., Sameshima, F., Ishikawa, T., Sumino, H. and Shinohara, N., 2011. New phased array and rectenna array systems for microwave power transmission research. *Proc. IMWS-IWPT 2011*, pp. 59-62.

Hui, S. Y. R. and Ho, W. C., 2005. A new generation of universal contactless battery charging platform for portable consumer electronic equipment. *IEEE Trans. Power Electron.*, 20 (3), pp. 620-627.

Hu, A. P., Liu, C. and Li, H. L., 2008. A novel contactless battery charging system for soccer playing robot. *IEEE 15th Int. Conf. on Mechatronics and Machine Vision in Practice*, pp. 646-650.

IEEE Standard for Safety Levels with Respect to Human Exposure to Radio Frequency Electromagnetic Fields, 3 kHz to 300 GHz. IEEE Std. C95.1, 1999.

Imura, T., Ichida, T. and Hori, Y., 2009. Basic experimental study on helical antennas of wireless power transfer for electric vehicles by using magnetic resonant coupling. *Proc. IEEE Vehicle Power and Propulsion Conf.*, pp. 936-940.

Jang, Y. T. and Jovanovic, M. M., 2003. A contactless electrical energy transmission system for portable-telephone battery chargers. *IEEE Trans. Ind. Electron.*, 50 (3), pp. 520-527.

Jeong, M. J., Park, K. H., Kim, J. M., Hwang, J. H., Hyung, C. H. and Kim, Y. T., 2012. Feasibility study on application of power transmission using magnetic coupling to body area network. *Electron. Lett.*, 48 (16), pp. 1013-1015.

Jiang, S. and Georgakopoulos, S. V., 2012. Optimum wireless powering of sensors embedded in concrete. *IEEE Trans. Antennas Propag.*, 60 (2), pp. 1106-1113.

Kalaris, A., Joannopoulos, J. and Soljacic, M., 2008. Efficient wireless non-radiative mid-range energy transfer. *Ann. Phys.*, 323 (1), pp. 34-48, January Special Issue 2008.

Kim, S., Ho, J. S. and Poon, A. S. Y., 2012. Wireless power transfer to miniature implants: Transmitter optimization. *IEEE Trans. Antennas Propag.*, 60 (10), pp. 4838-4845.

Kim, Y. H., Kang, S. Y., Lee, M. L., Yu, B. G. and Zyung, T. Y., 2009. Optimization of wireless power transmission through resonant coupling. *Proc. in Compatibility and Power Electron.*, pp. 426-431.

Kim, Y. and Ling, H., 2007. Investigation of coupled mode behaviour of electrically small meander antennas. *Electron. Lett.*, 43 (23).

Kim, J. W., Son, H. C., Kim, K. H. and Park, Y. J., 2011. Efficiency analysis of magnetic resonance wireless power transfer with intermediate resonant coil. *IEEE Antennas Wireless Propag. Lett.*, 10, pp. 389-392.

Kline, M., Izyumin, I., Boser, B. and Sanders, S., 2011. Capacitive power transfer for contactless charging. *Twenty-sixth Annual IEEE Applied Power Electron. Conf. and Exposition*, pp. 1398-1404.

Kurs, A., Karalis, A., Moffatt, R., Joannopoulos, J. D., Fisher, P. and Soljacic, M., 2007. Wireless power transfer via strongly coupled magnetic resonances. *Scienceexpress*, 317, pp. 83-86.

Kurs, A., Moffatt, R. and Soljacic, M., 2010. Simultaneous mid-range power transfer to multiple devices. *Appl. Phys. Lett.*, 96, pp. 044102-1-044102-3.

Lee, J. C. and Nam, S. W., 2010. Fundamental aspects of near-field coupling small antennas for wireless power transfer. *IEEE Trans Antennas Propag.*, 58, pp. 3442-3449.

Liu, C. and Hu, A. P., 2009. Steady state analysis of a capacitively coupled contactless power transfer system. *IEEE Energy Conversion Congress and Exposition*, pp. 3233-3238.

Liu, C. and Hu, A. P., 2011. Effect of series tuning inductor position on power transfer capability of CCPT system. *Electron. Lett.*, 47, pp. 136-137.

Liu, X. and Hui, S. Y. R., 2008. Optimal design of a hybrid winding structure for planar contactless battery charging platform. *IEEE Trans. Power Electron.*, 23 (1), pp. 455-463.

Liu, C., Hu, A. P. and Nair, N. K. C., 2009. Coupling study of a rotary capacitive power transfer. *IEEE Int. Conf. on Industrial Technology 2009*.

Liu, C., Hu, A. P. and Nair, N. K. C., 2011. Modelling and analysis of a capacitively coupled contactless power transfer system. *IET Power Electron.*, 4 (7), pp. 808-815.

Low, Z. N., Chinga, R. A., Tseng, R. and Lin, J. S., 2009. Design and test of a high-power high-efficiency loosely coupled planar wireless power transfer system. *IEEE Trans. Ind. Electron.*, 56 (5), pp. 1801-1812.

Matsumoto, H., 2002. Research on solar power station and microwave power transmission in Japan: Review and perspectives. *IEEE Microwave Mag.*, 3 (4), pp. 36-45.

Mcspadden, J. O., Fun, L. and Chang, K., 1997. A high conversion efficiency 5.8 GHz rectenna. *IEEE MTT-S Int Microwave Symp. Dig.*, pp. 547-550.

Mcspadden, J. O. and Mankins, J. C., 2002. Space solar power programs and microwave wireless power transmission technology. *IEEE Microwave Mag.*, 3 (4), pp. 46-57.

Mukhopadhyay, S. C., Gupta, G. S. and Lake, B. J., 2008. Design of a contactless battery charger for micro-robots. *Instrumentation and Measurement Technology Conf. Proc.*, pp. 985-990.

Olgun, U., Chen, C. C. and Volakis, J. L., 2011. Investigation of rectenna array configurations for enhanced RF power harvesting. *IEEE Antennas Wireless Propag. Lett.*, 10, pp. 262-265.

Park, S. B., Kim, W. K., Lee, J. S., Chung, Y. S. and Cheon, C. Y., 2008. A new receiver antenna for with buffer layer for wireless capsule endoscopy in human body. *IEEE AP-S Int. Symp. 2008*, pp. 1-4.

Park, J. M., Lee, S. H., Tak, Y. D. and Nam, S. W., 2012. Simple efficient resonant coupling wireless power transfer system operating at varying distances between antennas. *Microwave and Optical Technology Lett.*, 54 (10), pp. 2397-2401.

Park, J. M., Tak, Y. D., Kim, T. G., Kim, Y. W. and Nam, S. W., 2011. Investigation of adaptive matching methods for near-field wireless power transfer. *IEEE Trans. Antennas Propag.*, 59 (5), pp. 1769-1773.

RamRakhyani, A. K., Mirabbasi, S. and Chiao, M., 2011. Design and optimization of resonance-based efficient wireless power delivery systems for biomedical implants. *IEEE Trans. Biomed. Circuits Syst.*, 5 (1), pp. 48-63.

Sample, A. P., Meyer, D. A. and Smith, J. R., 2011. Analysis, experimental results, and range adaptation of magnetically coupled resonators for wireless power transfer. *IEEE Trans. Ind. Electron.*, 58 (2), pp. 544-554.

Shiba, K., Nagato, T., Tsuji, T. and Koshiji, K., 2008. Energy transmission transformer for a wireless capsule endoscope: Analysis of specific absorption rate and current density in biological tissue. *IEEE Trans. Biomed. Eng.*, 55 (7), pp. 1864-1871.

Shinohara, N., 2011a. Development of rectenna with wireless communication system. *Proc. 5th European Conf. Antenna Propag. (EUCAP' 11)*, pp. 4139-4142.

Shinohara, N., 2011b. Power without wires. *IEEE Microwave Mag.*, 12 (7), pp. S64-S73.

Shinohara, N., Fujiwara, J. and Matsumoto, H., 2000. Development of active phased array with phase-controlled magnetrons. *Proc. ISAP 2000*, Fukuoka, Japan, 2, pp. 713-716.

Shinohara, N. and Matsumoto, H., 1998. Experimental study of large rectenna array for microwave energy transmission. *IEEE Trans. Microwave Theory Tech.*, 46 (3), pp. 261-268.

Sodagar, A. M. and Amiri, P., 2009. Capacitive coupling for power and data telemetry to implantable biomedical microsystems. *Proc. 4th Int. IEEE EMBS Conf. Neural Eng.*, pp. 411-414.

Sun, T. J., Xie, X., Li, G. L., Gu, Y. K., Deng, Y. D. and Wang, Z. H., 2012. Integrated omnidirectional wireless power receiving circuit for wireless endoscopy. *Electron. Lett.*, 48 (15), pp. 907-908.

Sun, T. J., Xie, X., Li, G. L., Gu, Y. K. and Wang, Z. H., 2012. Rectigulator: A hybrid of rectifiers and regulators for miniature wirelessly powered bio-microsystems. *Electron. Lett.*, 48 (19), pp. 1181-1182.

Tak, Y. D., Park, J. M. and Nam, S. W., 2009. Mode-based analysis of resonant characteristics for near-field coupled small antennas. *IEEE Antennas Wireless Propag. Lett.*, 8, pp. 1238-1241.

Tak, Y. D., Park, J. M. and Nam, S. W., 2011. The optimum operating frequency for near-field coupled small antennas. *IEEE Trans. Antennas Propag.*, 59 (3), pp. 1027-1031.

Tang, S. C., Hui, S. Y. R. and Chung, H. S. H., 2000. Coreless planar printed-circuit-board (PCB) Transformers - A fundamental concept for signal and energy transfer. *IEEE Trans. Power Electron.*, 15 (5), pp. 931-941.

Tesla, N., 1904a. *Experiments with Alternate Current of High Potential and High Frequency*. New York: McGraw-Hill.

Tesla, N., 1904b. *The Transmission of Electrical Energy Without Wires (The Thirteenth Anniversary Number of the Electrical World and Engineer)*. New York: McGraw-Hill.

Tesla, N., 1914. U.S. Patent 1,119,732.

Vidhale, B. R. and Khanapurkar, M. M., 2012. Design of low cost and efficient strip line band pass filter for Bluetooth application. *Int. J. of Eng. Research and Applications*, 2 (4), pp. 2340-2345.

Wang, C. S., Stielau, O. H. and Covic, G. A., 2005. Design considerations for a contactless electric vehicle battery charger. *IEEE Trans. Ind. Electron.*, 52 (5), pp. 1308-1314.

Warnick, K. F., Gottula, R. B., Shrestha, S. and Smith, J. Optimizing power transfer efficiency and bandwidth for near field communication systems. *IEEE Trans. Antennas Propag.* (accepted for publication)

Yamanaka, K., Tuyama, Y., Ohtsuka, H., Chaki, S., Nakayama, M. and Hirano, Y., 2010. Internally-matched GaN HEMT high efficiency power amplifier for space solar power stations. *Proc. Asia-Pacific Microwave Conf.*, pp. 119-122.

Yoo, T. W. and Chang, K., 1992. Theoretical and experimental development of 10 and 35 GHz rectennas. *IEEE Trans. Microwave Theory Tech.*, 40 (6), pp. 1259-1266.

Yoon, I. J. and ling, H., 2010. Realizing efficient wireless power transfer using small folded cylindrical helix dipoles. *IEEE Antennas Wireless Propag. Lett.*, 9, pp. 846-849.

Zheng, H., Tnay, K., Alami, N. and Hu, A. P., 2010. Contactless power couplers for respiratory devices. *IEEE Int. Conf. on Mechatronics and Embedded Syst. and Applications*, pp. 155-160.

Zhu, C. B., Yu, C. L., Ma, R. and Cheng, H. X., 2008. Simulation and experimental analysis on wireless energy transfer based on magnetic resonances. *IEEE Vehicle Power and Propulsion Conf.*